Chronic Ethanol Exposure Produces Sex-Dependent Impairments in Value Computations in the Striatum

Yifeng Cheng[1,5]*, Robin Magnard[1], Angela J. Langdon[2], Daeyeol Lee[1,3,4,5], and Patricia H. Janak[1,4,5]*

[1]Department Psychological and Brain Sciences, Krieger School of Arts and Sciences, Johns Hopkins University, Baltimore, MD;
[2]Intramural Research Program, National Institute of Mental Health, National Institutes of Health, Bethesda, MD;
[3]Zanvyl Krieger Mind/Brain Institute, Krieger School of Arts and Sciences, Johns Hopkins University, Baltimore, MD;
[4]Department of Neuroscience, Johns Hopkins University School of Medicine, Baltimore, MD;
[5]Kavli Neuroscience Discovery Institute, Johns Hopkins University, Baltimore, MD.

*Corresponding authors (patricia.janak@jhu.edu; ycheng62@jhu.edu)

Value-based decision-making relies on the striatum, where neural plasticity can be altered by chronic ethanol (EtOH) exposure, but the effects of such plasticity on striatal neural dynamics during decision-making remain unclear. This study investigated the long-term impacts of EtOH on reward-driven decision-making and striatal neurocomputations in male and female rats using a dynamic probabilistic reversal learning task. Following a prolonged withdrawal period, EtOH-exposed male rats exhibited deficits in adaptability and exploratory behavior, with aberrant outcome-driven value updating that heightened preference for chosen action. These behavioral changes were linked to altered neural activity in the dorsomedial striatum (DMS), where EtOH increased outcome-related encoding and decreased choice-related encoding. In contrast, female rats showed minimal behavioral changes with distinct EtOH-evoked alterations of neural activity, revealing significant sex differences in the impact of chronic EtOH. Our findings underscore the impact of chronic EtOH exposure on adaptive decision-making, revealing enduring changes in neurocomputational processes in the striatum underlying cognitive deficits that differ by sex.

Introduction

Value-based decision-making is a fundamental cognitive process that involves evaluating the potential outcomes of different actions to choose the most beneficial one. This process is crucial for adaptive behavior and relies heavily on neural computations in the striatum, a key brain region for encoding various decision-related signals, including those related to choice, rewards, and value (1-9).

Chronic ethanol (EtOH) exposure is known to enduringly disrupt learning and cognition in humans (10-13) and rodents (14-16), and to profoundly affect the brain, particularly in regions involved in decision-making and reward processing, such as corticostriatal pathways. Previous research has demonstrated that EtOH alters striatal cell signaling and corticostriatal plasticity (17-20), especially in the dorsomedial striatum (DMS) (18-20), a region critical for economic decision-

making (4, 9, 21, 22), reward learning (1-3, 8, 23, 24), and goal-directed action planning (25, 26). However, how chronic alcohol exposure affects specific decision processes underlying reward learning and disrupts systems-level striatal dynamics of these decision processes remains underexplored.

Many psychiatric diseases, including alcohol use disorders, disproportionately affect one sex over the other, underscoring the importance of considering sex differences in research (27). Studies indicate that males and females exhibit distinct patterns of alcohol consumption and susceptibility to alcohol-related disorders (28), potentially driven by differences in neurobiology (29, 30). Moreover, males and females have been shown to exhibit distinct behavioral responses and motivational levels in reward learning (5, 31). These sex differences may extend to the effects of alcohol on decision-making and the underlying neural mechanisms. Thus, it is important to understand how chronic ethanol exposure influences striatal encoding of reward learning signals in a sex-dependent manner, as these neural changes can lead to persistent impairments in decision-making.

To address these questions, we trained both male and female rats that had undergone a period of EtOH-dependence in a dynamic probabilistic reversal learning (dynaPRL) task. During the standard reversal learning (PRL) task, animals experience alternating blocks where the reward probabilities symmetrically switch between two options. Therefore, the uncertainty in the outcome, referred to as expected uncertainty (32, 33), is fixed and the transition between different reward probabilities are somewhat predictable resulting in a relatively low level of unexpected uncertainty (32, 34). By contrast, the dynaPRL task requires rats to assess reward probabilities under varying levels of expected uncertainty, corresponding to a higher level of unexpected uncertainty. Using this task, we observed EtOH-induced changes across multiple behavioral measures, including altered exploration-exploitation trade-offs and reversal deficits in more uncertain environments, which were more pronounced in male rats than in female rats. Using a reinforcement learning framework, we found that both EtOH-exposed male and female rats showed enhanced value updating after rewards, but only males exhibited specific alterations after no reward, offering a potential computational explanation for the observed deficits. Additionally, single-unit recordings in the DMS revealed reduced encoding of choice, state value, and policy, alongside an enhanced encoding of outcome and chosen value in male rats with an EtOH history. Notably, our observations revealed that female rats displayed a distinct pattern of encoding for decision variables compared to males, irrespective of EtOH history, and EtOH history altered neural encoding in females differently than in males, underscoring significant sex-specific effects. Together, these findings reveal behavioral and neural mechanisms underlying adverse effects of chronic EtOH exposure during protracted withdrawal, highlighting marked sex differences in the impact of EtOH on value-based decisions and decision-related striatal neural activity.

Results

Protracted withdrawal from chronic EtOH exposure produces a sex-specific behavioral pattern

To investigate whether chronic EtOH exposure disrupts decision-making beyond the phase of acute withdrawal (i.e., >1 week), we used a well-validated chronic intermittent EtOH (CIE) vapor procedure that results in blood EtOH concentrations (BEC) greater than 150 mg/dl thereby modeling EtOH dependence (**Figure 1A**) (14, 35). Rats were first trained on a standard probabilistic reversal learning (PRL) task and then underwent cycles of EtOH vapor or air exposure and withdrawal for four weeks (16 hrs/day, 5 days/wk; no sex difference in BEC $t_{(11)} = -1.05$, $p = 0.32$), with group assignment balanced for PRL performance. Following 10-15 days of

withdrawal, performance on the standard PRL task was reassessed (**Figure S1A**). This task required water-restricted rats to earn a drop (33 µl) of a 10% sucrose solution by choosing between left and right levers that delivered a reward with either a 70% or a 10% probability; these reward probabilities for the left and right levers repeatedly switched within a session (**Figure 1B and S1B**). Consistent with previous studies (36, 37), during this standard PRL task, we did not observe any significant differences in reversal learning after block switches when comparing within-subject performance before and after CIE exposure (**Figures S1C-1G**), nor between EtOH and air controls for either male or female rats (**Figures S1C-1G**). To further understand whether CIE exposure could induce behavioral changes in this task, we employed a Support Vector Machine analysis (SVM) to decode group membership from a high-dimensional dataset consisting of 20 behavioral measures gathered during pre- and post-reversal phases in EtOH rats and their air controls (**Figure S2A**). We found that trained SVM models could not identify either group labels or sex labels in this PRL task above chance levels (**Figure S2B**). These findings indicate that rats did not express significant EtOH-induced performance changes within the standard PRL task.

To further explore possible effects of chronic EtOH on decision making, we next modified the task to increase levels of uncertainty (38, 39). We introduced a three-block design with reward probabilities that varied in the contrast between left and right lever probabilities (80:10, 60:30, and 45:45; **Figure 1B and 1C**), converting the standard PRL task into a dynamic PRL task (dynaPRL). This design created blocks with varying levels of expected uncertainty (32, 33) in predicting action-outcome probabilities, while the unpredictable transitions between blocks introduced unexpected uncertainty (32, 34) (**Figure 1C**). Together, these uncertainties in the dynaPRL task likely create a greater cognitive challenge for rats, potentially providing a more sensitive measure of EtOH-induced cognitive changes than the traditional PRL task by placing added demands on cognitive flexibility. This conclusion is supported by comparisons of behavior between the PRL and the dynaPRL (**Figure S1G-L)**. Individual rats in both air and EtOH groups adjusted their choice behavior in response to block transitions within the dynaPRL task (**Figure 1D**). Applying the SVM model to the same behavioral features used in the analysis for the standard PRL task, we found the model could correctly identify group (air vs. EtOH) and sex labels from the dynaPRL behavioral data with a prediction precision (63.29%) significantly higher than chance levels (25%; $p < 0.001$). The trained SVM decoder almost never (<0.001% probability) misclassified male and female subjects (**Figures 1E, 1F and S2C-S2G**). Moreover, the decoding accuracy for EtOH treatment vs. air was significantly higher than chance for male but not female rats (**Figure 1F**). Using Uniform Manifold Approximation Projection (UMAP), we found that the data were distinctly segregated for male EtOH and air rats in a 2D low-dimensional space with an accuracy (~75%) similar to the SVM decoding of group membership (**Figure 1G**).

Taken together, these results indicate that the impact of prior chronic EtOH exposure can be detected in male rats many weeks (>10 wks) after the last EtOH exposure through multivariate analysis of high dimensional behavioral measures during the more challenging dynaPRL decision-making task.

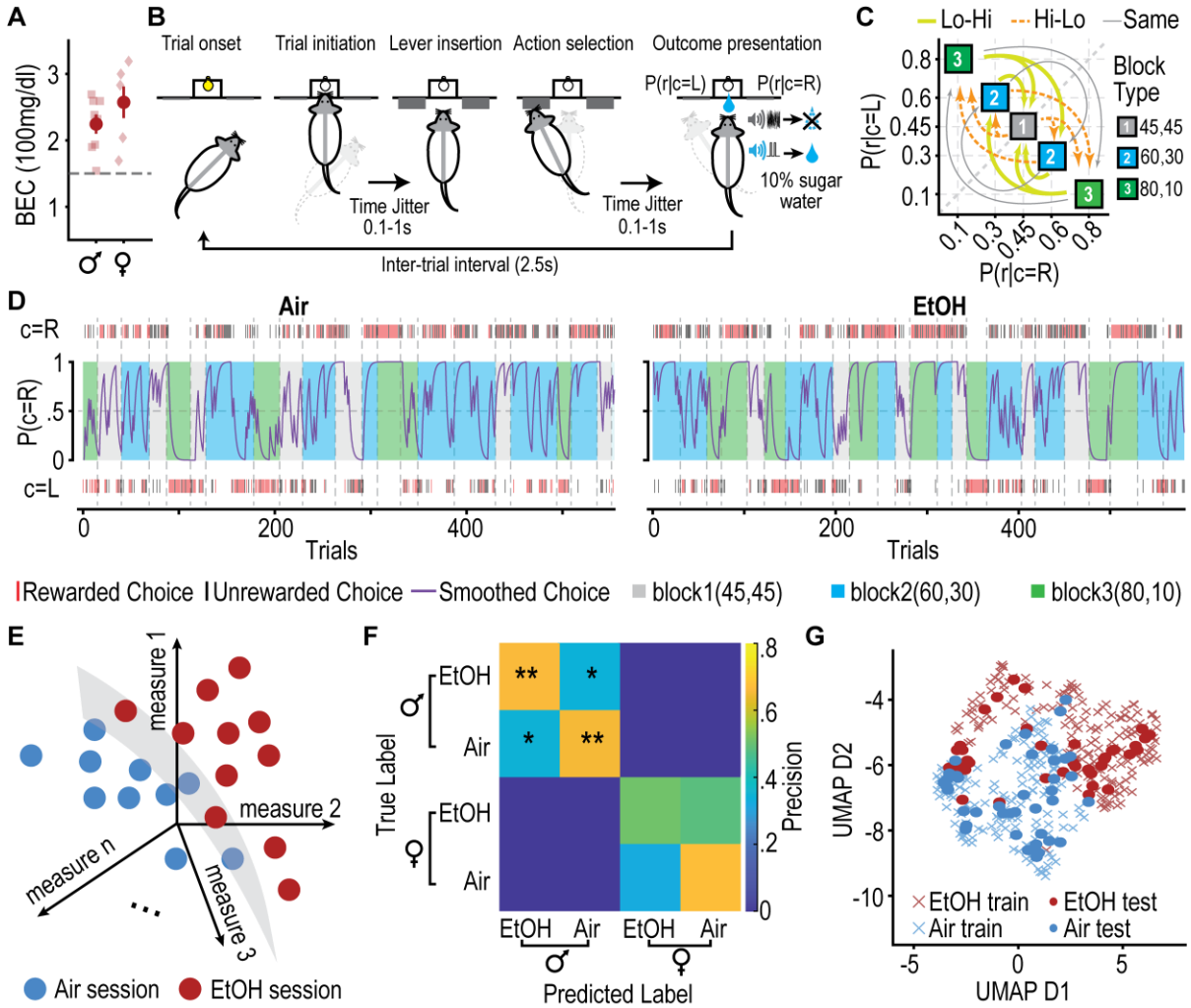

Figure 1. EtOH-exposed rats exhibit a distinct behavioral pattern in the dynaPRL task. (**A**) Blood ethanol (EtOH) concentrations (BEC) of male and female rats during EtOH vapor exposure. (**B**) dynaPRL trial structure. A rewarded choice is indicated by a clicker sound followed by sucrose; an unrewarded choice is indicated by white noise. P(r|c=L) or p(r|c=R) is the reward (r) probability given that the choice (c) is left (L) or right (R) side. (**C**) Choice reward probabilities for dynaPRL task. Block transitions are categorized into three types: low to high (LH) challenge, high to low (HL) challenge, and same to same (no difference, ND), denoted as lines with distinct colors, styles and thickness. (**D**) Example choice behavior of air- and EtOH-exposed rats. Choices are shown as red (rewarded) or grey (unrewarded) hashmarks. A moving average (5-trial window) estimates the probability of choosing the right lever, P(c=R). (**E**) Schematic of a hyperplane separating EtOH and air sessions in multidimensional behavioral space, representing distinct patterns. (**F**) Confusion matrix for the SVM multiclass classifier aggregating from 1000 iterations for decoding both group and sex for n = 13 EtOH rats (8 male, 5 female) and 14 air controls (9 male, 5 female). Diagonal entries indicate probability of correct predictions; off-diagonal entries represent misclassifications. *p < 0.05, **p < 0.01, Monte Carlo significance tests. (**G**) A UMAP transformation of high dimensional data onto a 2D space.

Chronic EtOH exposure slows adaptive learning and reduces exploration in males

The SVM analysis showed that behavior of male EtOH-exposed rats in the dynaPRL task differed from control rats. To understand the basis for this difference, we examined how EtOH and air rats adjusted their choice behaviors in response to changes in reward probabilities after a block

switch. The uncertainty associated with each block can be quantified by entropy, which measures the unpredictability of outcomes: 1.04 bits for the 45-45 block (block 1), 0.96 bits for the 60-30 block (block 2), and 0.59 bits for the 80-10 block (block 3). Transitions between these blocks introduce unexpected uncertainty (32, 34), which we categorized based on the relative uncertainty levels before and after the switch: for example, transitions from lower to higher expected uncertainty were labeled as Low-High, and from higher to lower as High-Low (**Figure 1C**).

During block switches, we analyzed the likelihood of selecting the action that was advantageous before the transition. We found that rats across all sex and treatment groups displayed unique adaptive learning responses based on the type of block transition (**Figure S4A and 4E**), indicating that unexpected uncertainty in the dynaPRL task influences choice behavior. When examining the EtOH effect on learning performance across different types of unexpected uncertainty, we found that during Low-High transitions (**Figure 2A**), EtOH-exposed male rats had a higher probability of persevering with their preferred choice from the previous block during the initial trials after switching to the new block. This was supported by a two-way mixed-effect ANOVA, which revealed a significant interaction between treatment group and trials in males (**Figure 2B**; $F_{(16,255)} = 1.925$, $p = 0.016$). To quantify adaptive learning performance in male rats, we fit a single-exponential decay model to the probability of choosing the previously preferred action across the first 12 trials after the block transition (**Figure 2C**). While there was no difference in pre-block switch asymptotic value (*a)* or the magnitude of change in learning new action-outcome contingency after the block switch (*d*) (**Figures 2D and 2E**), we observed a lower adaptation rate (λ) in EtOH males compared to the same-sex controls (**Figure 2F**; $t_{(15)} = -2.36$, $p = 0.016$). Given that the inverse of λ ($\tau = 1/\lambda$) corresponds to the time constant of the rat's learning in a new block, this indicates that EtOH rats required more experience to adapt to a new contingency in a highly ambiguous environment (**Figure 2G**; $t_{(15)} = 2.3$, $p = 0.036$; **Figure S4A**). Notably, these effects were not observed during block transitions from high to low uncertainty (High-Low), at the same uncertainty level before and after block transitions (same), or when all trial types were combined (**Figures S3B-3D and S4A**). In contrast, we found that female EtOH and air rats exhibit identical performance across all transition types (**Figure S3G-SJ and S4E**). Thus, consistent with the SVM analysis, the impact of EtOH on adaptive learning dynamics was present only in male rats, and only when they face a sudden transition to high uncertainty. To examine choice behavior later in a block after rats are expected to have acquired the new contingencies, we focused on behavior after 12 trials from block switch and assessed how much choice probability deviated from local reward rate yielded by the choice ('matching behavior') (40). Male, but not female, EtOH rats aligned their choices with local reward rates more tightly than same-sex control rats (**Figure S5**), again supporting sex differences in choice behavior in this task.

To understand these differences, we investigated whether and how EtOH might differentially impact choice strategies in male and female rats. We analyzed stay probabilities in two phases, the early adaptive learning phase, including trials 2 to 7 after transitioning to a new block, and the late performance phase of the current block, spanning the last 6 trials before block switch. We found that male EtOH rats were more likely to repeat the same choice in two consecutive trials, especially in the early phase following a switch (**Figure 2H**; $z_{(464)} = -2.36$, $p = 0.018$), but less in the late phase after rats have adapted to the contingency change, as shown by measures of stay probabilities and the differences between win-stay and lose-shift probabilities (**Figures 2H-2J and S6A-S6H**). This behavior was sensitive to the receipt or omission of reward; EtOH rats exhibited higher stay probabilities after reward omission, but not after reward receipt,

during Low-High transitions (**Figure 2I**; main effect of group, $F_{(1, 463)} = 10.625$, $p = 0.001$; outcome × group interaction, $F_{(1, 463)} = 4.5$, $p = 0.035$), resulting in a greater tendency for win-stay behavior and less tendency for lose-shift behavior (**Figure 2J**; $z_{(464)} = -2.81$, $p = 0.005$). By contrast, female EtOH exposed rats did not show alterations in win-stay lose-shift behavioral strategies (**Figures S6I-S6P**). Notably, EtOH-naive male rats also had higher stay probabilities and a greater tendency for win-stay behavior than EtOH-naive female rats (**Figures S2F**).

Collectively, these results demonstrate that chronic EtOH exposure significantly impacts outcome-driven action strategies in male rats, favoring a shift from switch to stay and enhancing matching behaviors, i.e., a tendency for greater exploitation and less exploration, resulting in a sex-dependent reduction in cognitive flexibility during a dynamic decision-making task.

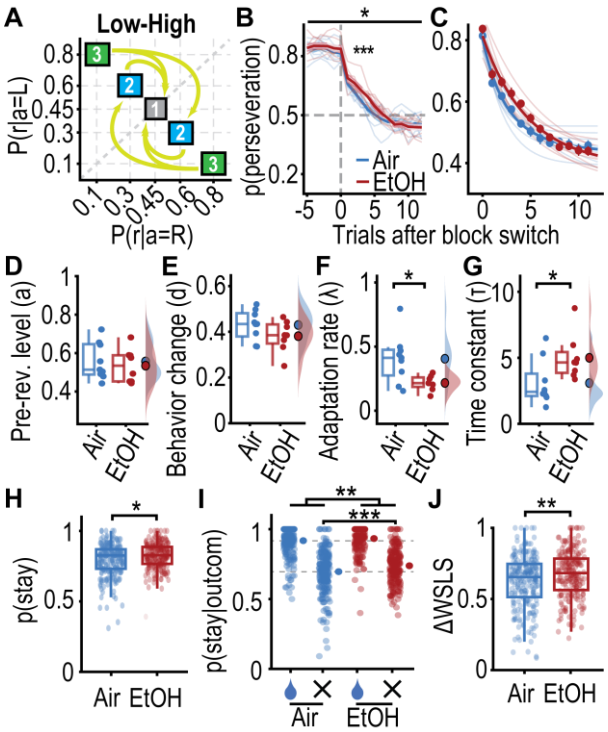

Figure 2. Chronic EtOH exposure alters choice behavior of male rats in ambiguous environments. (**A**) Diagram of block switching in Low-to-High uncertainty transitions. **(B)** Probability of choosing the pre-switch preferred lever in Low-to-High transitions. Bold lines represent group averages; faded lines represent individual rats. Dashed vertical line marks block switch (t=0). (**C**) A single exponential decay model estimates performance in learning new action-outcome contingency. Bold lines show average model fits; dots depict true mean data from B. Faded lines indicate individual rat model fits. **(D-G)** Estimated parameters from C. The box plot depicts the median, 25th, and 75th percentile of parameter values for each group. Dots next to the box plot are values from individual rats. Cloud plots on the right side of panels depict the data distribution. Dots on cloud plots are the mean of parameter values. *p < 0.05, t test. n = 9 Air rats, 8 CIE rats for B-G. (**H**) Stay probability during Low-High transitions. (**I**) Stay probability given reward (water drop) or no reward (X) on the prior trial, during Low-High transitions. Dots next to scatter plots represent data means. Standard errors are vertical lines but are too small to visualize on the graph. Horizontal dashed lines represent the means of air group. (**J**) Difference (Δ) between probability of stay given reward (win-stay, WS) and probability of shift given no reward (lose-shift, LS), during Low-High transitions. *p < 0.05 and ***p < 0.001, two-way mixed-effect ANOVA followed by post hoc test with Bonferroni correction for A and I. *p < 0.05 and **p < 0.01, Wilcoxon rank-sum test for H and J. N = 241 sessions from 9 air rats, 229 sessions from 8 EtOH rats for H-J.

Chronic EtOH exposure alters outcome-specific value updating in male rats

To better understand the reward learning processes underlying the observed effects of EtOH exposure on decision-making, we fit several reinforcement learning (RL) models to the trial-by-trial choice and reward data. We found that a Q-learning model with differential learning rates (model 2, Q-DFLr) outperformed all other candidate models (**Figure S7A**). Q-DFLr has four distinct parameters controlling the updating of the value function: α^+ and α^- for the rate of updating the value of chosen actions when the outcome is reward or no reward, respectively, and θ^+ and θ^- for the rate of discounting the value of unchosen actions in an outcome-dependent fashion (**Figure 3A**). To assess the group-level differences between the EtOH and air groups across these RL parameters, we constructed a hierarchical model wherein the distributions of individual parameters for each rat are determined by the group-level hyperparameters. These hyperparameters encompass the means of the distributions for each parameter, the mean differences (δ) between air and EtOH groups for each parameter, and the variances of each parameter's distribution. The posterior density of these hyperparameters was estimated through sampling using Hamiltonian Markov Chain Monte Carlo (HMC) methods. We observed a rightward shift in the posterior distributions of the group difference parameter, δ, for the learning rate α^+ in both male and female rats (**Figure 3B**). Using directed Bayes Factor (dBF) to assess the strength of this shift, we found that the rewarded learning rate changed relatively similarly across the sexes, with α^+ being approximately 6 times more likely to increase than decrease in males, and 5 times more likely in females, following EtOH pre-exposure compared to same-sex controls (**Figure 3B**; dBF = 6.1 for male and 5.5 for female). Notably, the unrewarded learning rate, α^-, was more likely to increase following EtOH exposure only in females (**Figure S6B**; dBF = 2.18), but not in males (**Figure S6B**; dBF < 1). Additionally, we found that the discounting parameter, θ^-, exhibited a pronounced rightward shift in males, where it was approximately 8 times more likely to increase than decrease after EtOH pre-exposure (**Figure 3C**; dBF = 8.35). In contrast, the likelihood of θ^- increasing after EtOH exposure was considerably lower in females (**Figure 3C**; dBF = 1.54). All other parameters showed only small differences between the two groups for both sexes (**Figure S7B**; all dBFs < 1).

We then used the best-fit parameters to simulate choice behavior within the original block structure used in the experiment and analyzed the probabilities of perseveration for each block transition type. We found that the simulated data partially recapitulated the EtOH-induced adaptive learning deficits observed in the empirical data from male, but not female, rats when transitioning from a low to a high uncertainty block, but not for other types of block transitions (**Figures 3D and S7C**). Collectively, these data suggest that chronic EtOH exposure preferentially alters reward learning in males relative to females by strongly enhancing omission-based forgetting of unselected options, along with enhancing outcome-based updating of selected actions, that together bias action-selection towards previously reinforced choices. These results provide an algorithmic explanation for the sex-dependent changes in choice behavior we observed.

Sex-dependent effects of EtOH exposure on DMS activity related to actions and outcomes

Our behavioral analyses and RL model fitting indicated that male and female EtOH rats exhibit distinct outcome-dependent value updating. This suggests that EtOH might differentially alter neural processes related to action and outcome signals. Therefore, we sought to examine the impact of EtOH on DMS neural dynamics within the dynaPRL task. We recorded 504 and 247 single units in the DMS from male EtOH and air control rats, respectively, and 354 and 347 single units from female EtOH and air control rats, respectively (**Figure S8A-S8C**). For the vast majority

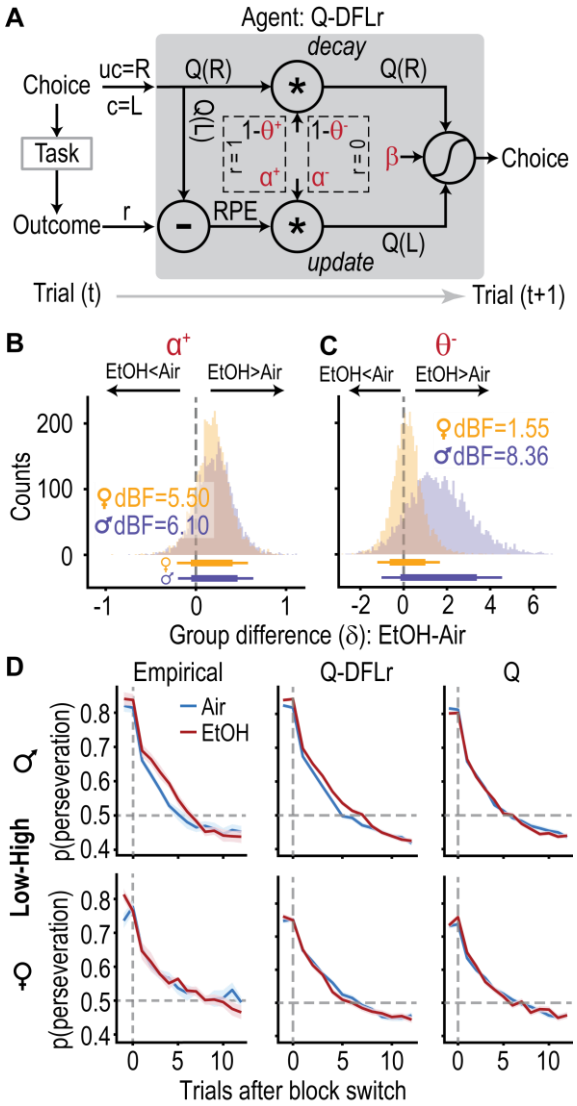

Figure 3. EtOH exposure enhances positive feedback-mediated learning rates and negative feedback-mediated forgetting rates. (**A**) Schematic of the value updating processes by the best-fitting RL agent, Q-DFLr. In this example, the agent updates chosen, Q(L), and unchosen Q(R), action values based on reward prediction error (RPE) after receiving positive (reward, r=1) or negative (no reward, r=0) feedback. Chosen values update with learning rates (α^+ for reward, α^- for no reward), while unchosen values decay with forgetting rates (θ^+ for reward, θ^- for no reward). Updated values guide choices via a softmax function. (**B,C**) Hamiltonian Markov chain Monte Carlo (HMC)-sampled posterior densities of group difference, δ, between EtOH- and air-exposed male (♂) and female (♀) rats in positive feedback-mediated learning rates (α^+) in (B) and negative feedback-mediated forgetting rates (θ^-) in (C), across group-level hyperparameters. The rightward arrow indicates that parameter values are higher in EtOH compared to air, while the leftward arrow indicates that parameter values are lower. Bottom horizontal lines represent the 80% and 95% highest density interval (HDI). dBF, directed Bayes factor. Posterior densities aggregated from 1000 times Monte Carlo sampling. (**D**) Choice probability of the initially preferred lever in Low-High transitions. Data in left panels are empirical (reproduced from Figure 1G for male, Figure S4G for female); middle and right panels depict simulated data, generated using the best-fitting parameters from Q-DFLr and Q models, respectively. Each line represents an average of 20 simulations.

of recorded striatal neurons, their firing rates were lower than 18 Hz (92% in males and 96% in females) (**Figure S8D and S8E**). All neurons are included in the following analyses (see Methods).

Using multiple linear regression models, we examined how neural activity in different epochs throughout the trial was affected by an animal's action, the outcome of the action, and the interaction of the selected action and its outcome, for both the current trial (t) and the previous trial (t–1) and compared the significance of this modulation at the group level using a generalized linear mixed-effects models (GLMM). Choice direction (ipsi- or contra-lateral to the recorded hemisphere) signals reflecting the action made on the current trial (**Figures 4A and 4B**), but not the previous trial (**Figures S9A and S9B**), were apparent in both groups and sexes throughout much of the trial. In both EtOH-exposed and control rats, an increase in choice-modulated neurons was observed from the intertrial interval to outcome presentation, with no sex-specific differences. Following the onset of outcome, female rats showed higher choice encoding than males, regardless of EtOH history ($p = 0.0022$, main effect of sex). Additionally, a significant interaction between sex and EtOH treatment on neural encoding of choice direction during the outcome period was

found ($p = 0.032$), corresponding to fewer choice-modulated neurons in EtOH-exposed males relative to air controls ($p = 0.027$, main effect of treatment), but more choice-modulated neurons in EtOH-exposed females than air controls, especially early in the outcome period ($p = 0.0096$, interaction between treatment and time).

When examining the impact of trial outcomes on neural activity, we again found sex-dependent differences in EtOH and air groups during the outcome period itself ($p = 0.013$, interaction among treatment, sex and time). In EtOH males, a higher proportion of DMS neurons (~80%) was modulated by the outcome compared to air controls (~50%) (**Figures 4C and 4D**; $p < 0.0001$, main effect of treatment and interaction between treatment and time). By contrast, in females, both EtOH and air groups showed similar proportions of neurons (~75%) immediately after outcome onset, but the outcome signal diminished more slowly in EtOH females ($p = 0.0040$, interaction between treatment and time). To further dissociate this EtOH-driven effect in both sexes, we analyzed neuronal firing rates following rewarded and unrewarded outcomes and found a greater proportion of neurons modulated by both outcome types in EtOH males compared to controls (**Figures S10A and S10B**; chi-squared test, $p < 0.0001$), while females showed no significant treatment effect (**Figures S10C and S10D**). We also analyzed the impact of the outcome received on the previous trial on neural firing, and found the prior reward was significantly encoded throughout the current trial, with pronounced sex-dependent differences observed during the ITI period in EtOH versus control groups ($p = 0.0069$) (**Figures S9C and S9D**). Specifically, previous outcome signals diminished faster in EtOH males and slower in EtOH females compared to their respective controls ($p < 0.0001$, interaction between treatment and time in both groups).

Lastly, we found that EtOH differentially impacted encoding dynamics of the action-outcome (A-O) interaction (a proxy for contingencies) in DMS neurons recorded from males compared to females (**Figures 4E and 4F**; $p = 0.00098$, interaction among treatment, sex, and time). The encoding of the action-outcome interaction was more prominent at the start of outcome presentation in EtOH males, whereas it became more pronounced toward the end in air controls ($p = 0.044$, interaction between treatment and time). By contrast, no significant differences were observed between neural populations recorded from EtOH and controls in females. This neural encoding of A-O interaction was detected only when analyzing current trial events (**Figures S9E and S9F**).

Collectively, these results demonstrate that EtOH pre-exposure differentially modulates neural encoding of choice direction and outcome signals during outcome presentation in a sex-dependent manner. Additionally, EtOH impacts the dynamics of action-outcome interaction encoding in males, suggesting that EtOH alters the temporal processing of action-outcome contingencies in a sex-dependent manner.

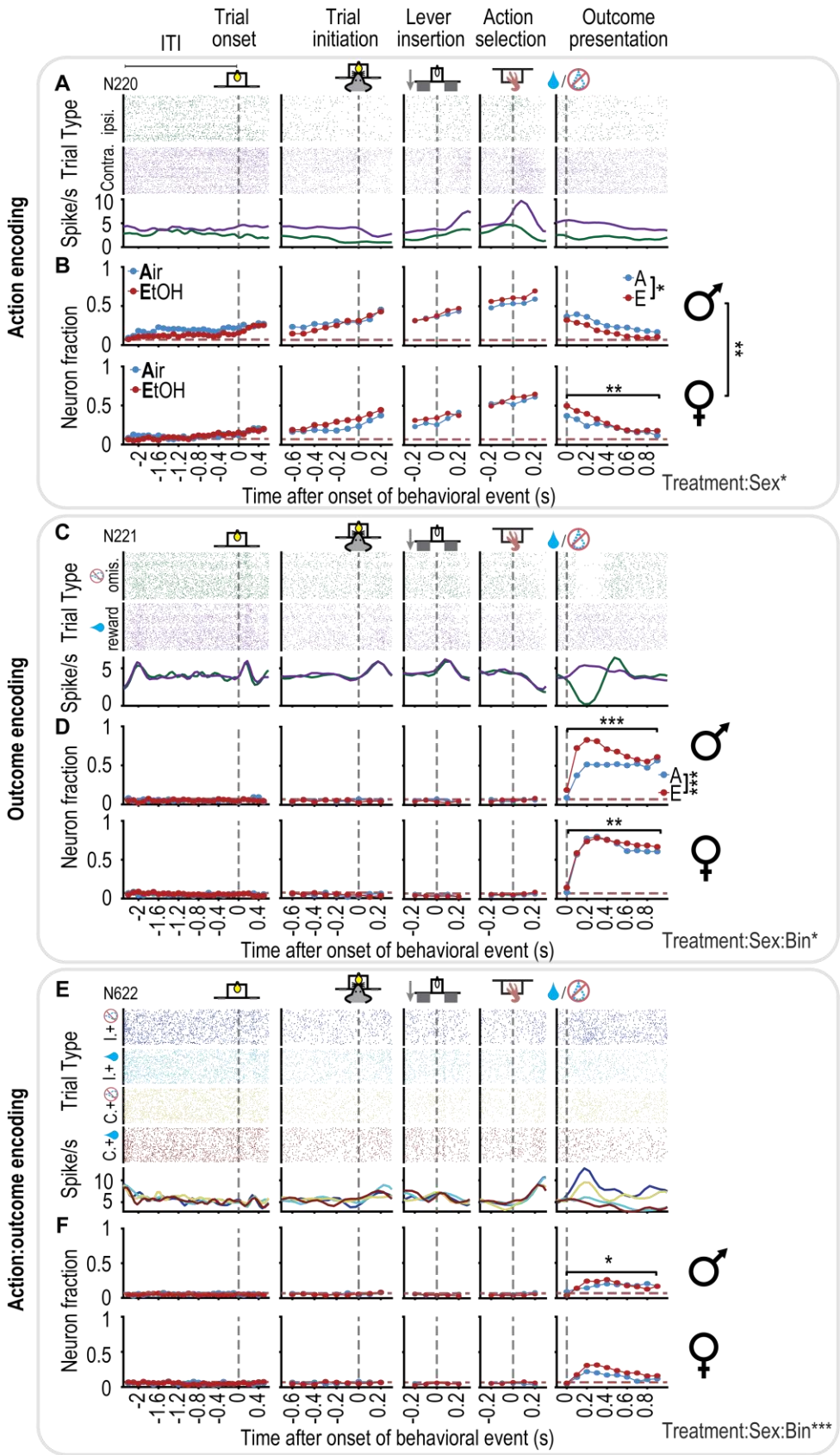
ITI
Trial onset
Trial initiation
Lever insertion
Action selection
Outcome presentation
Action encoding
A
N220
Trial Type
ipsi.
Contra.
Spike/s
B
Air
EtOH
Neuron fraction
Time after onset of behavioral event (s)
Treatment:Sex*
Outcome encoding
C
N221
omis.
reward
D
Treatment:Sex:Bin*
Action:outcome encoding
E
N622
I.+
C.+
F
Treatment:Sex:Bin***

Figure 4. **EtOH exposure alters encoding of action and outcome during outcome presentation.** (**A, C, E**) Example DMS unit shows spike activity correlated with A) action side, C) outcome (reward or omission), E) interaction of choice and outcome (action:outcome) in the current trial. At top are spike raster plots, trials are grouped by A) choice side, ipsilateral (ipsi) or contralateral (contra) to the recording site, C) outcome, rewarded (reward) or unrewarded, and E) distinct contingencies of ipsilateral choice without reward ('I' and no water drop), ipsilateral choice with reward ('I' and water drop), contralateral choice without reward ('C' and no water drop), and contralateral choice with reward ('C' and water drop). Spike density functions generated by applying a Gaussian kernel (δ = 100 ms) to the corresponding spike trains. (**B, D, F**) Fraction of neurons with activity significantly modulated by the current trial B) action, D) outcome, and F) action:outcome interaction across all trial landmarks, including intertrial interval (ITI) prior to trial onset, trial initiation, lever insertion, action selection, and outcome presentation. Horizontal dashed lines indicate chance level (binomial test, $\alpha = 0.05$). *$p < 0.05$, **$p < 0.01$, ***$p < 0.0001$, logistic regression with Generalized Linear Mixed-Effect Model for B,D and F. n = 247 neurons from 9 air male rats, 504 neurons from 8 EtOH male rats, 347 neurons from 5 air female rats, and 354 neurons from 5 EtOH female rats.

Chronic EtOH exposure persistently alters value signals in the DMS in a sex-dependent manner

Next, we evaluated whether EtOH impacted encoding of value signals in the DMS during the action selection process, defined as the time period from the beginning of the ITI until a lever press. Specifically, we sought to quantify the strength and time course of striatal activity related to two orthogonal combinations of the action values (41) estimated by the best-fitting RL model (model 2, Q-DFLr). The first variable is the summation of the two available action values, ΣQ, which represents the richness of the recent environment and roughly corresponds to the so-called state value. The state value is likely to be important environmental information for inferring the block type. Although each block has the same average reward probability, the local reward rate reflects the uncertainty level of the block (**Figure S11**). Thus, a better representation of state value might aid rats in inferring their current environment. The second variable corresponds to the difference between the two available action values, ΔQ, which is monotonically related to the probability of selecting one action over the alternative and is referred to as the policy signal. We analyzed neural firing rates, aligned with either trial onset (including ITI), trial initiation, lever insertion, or lever press, as linear functions of ΔQ and ΣQ, while accounting for the effects of choice and chosen action value in the regression analysis.

We found that ~40% of striatal neurons across all groups and sexes exhibited changes in spike rate in response to the ΣQ (state value) at the beginning of the ITI, which gradually diminished to chance levels (binomial test, $\alpha = 0.05$) around the lever insertion period (**Figures 5A, 5D, and 5G**). During the ITI period, EtOH exposure modulated the neural encoding dynamics of state value in a sex-dependent manner ($p < 0.0001$, interaction among treatment, sex, and time). In males, the proportion of neurons encoding state value decreased more rapidly in EtOH-exposed rats compared to controls ($p < 0.0001$, **Figure 5D**), while no significant differences were observed in females (**Figure 5G**). In addition, we observed approximately 20% of striatal neurons encoded action policy (ΔQ) at the beginning of the ITI across all groups and sexes (**Figures 5B, 5E, and 5H**). Throughout the ITI period and trial onset, EtOH selectively altered striatal encoding of policy in neural populations recorded from males but not females ($p = 0.0016$, interaction between treatment, sex, and time). In EtOH male rats, the proportion of policy-encoding neurons decreased faster than in their air-exposed controls (**Figure 5E**; $p = 0.00064$, interaction between treatment

and time bin), whereas no significant differences in policy encoding were observed between EtOH and air-exposed females (**Figure 5H**).

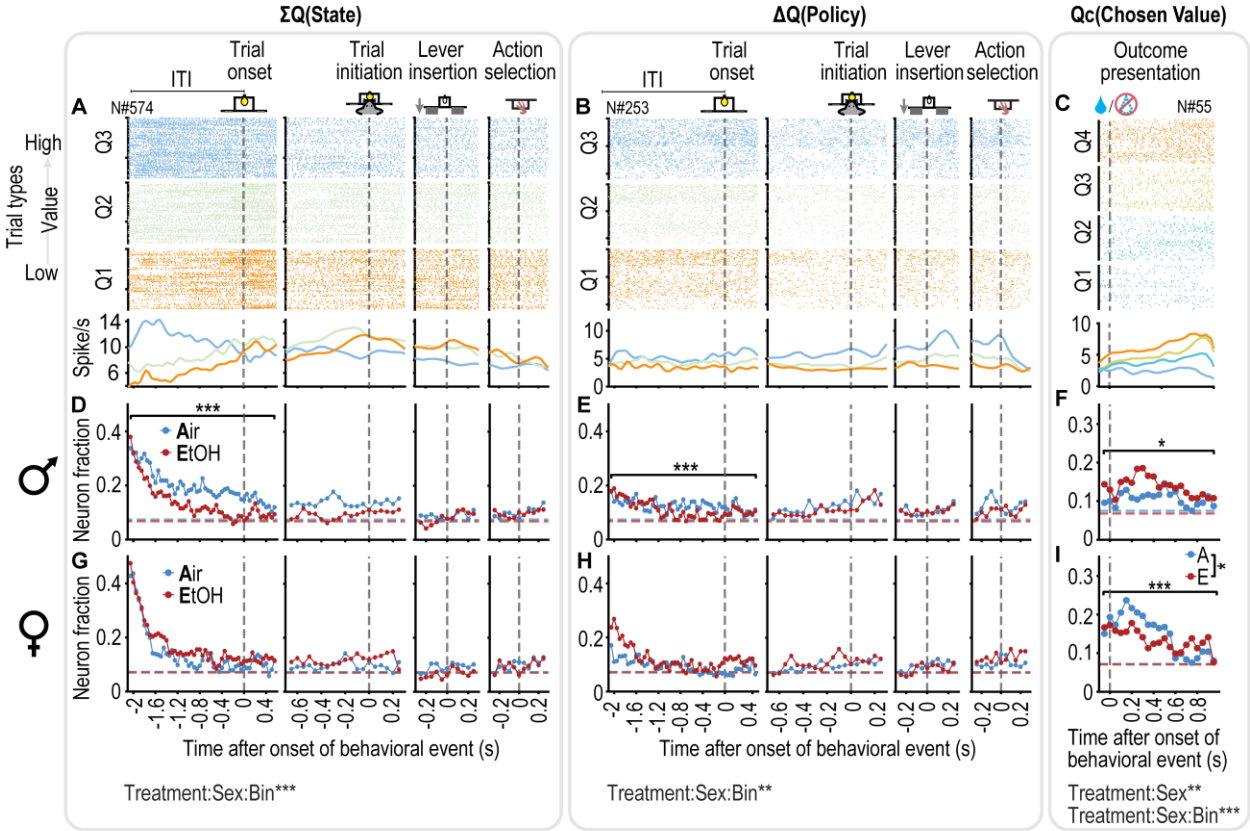

Figure 5. EtOH exposure alters striatal value encoding. (**A-C**) Example DMS unit shows spike activity correlated with value of state, ΣQ (A), and policy value, ΔQ (B), during action planning (i.e., inter-trial interval (ITI), trial onset, trial initiation, lever insertion) and action selection, as well as chosen value (C) during outcome presentation. In top raster plots in panels A and B, trials are grouped into three quantiles of the value (Q1, Q2, and Q3), with each quantile representing 33.3% of the data. In top raster plots in panel C, trials are grouped into quartiles of the chosen action value (Q1, Q2, Q3, and Q4), with each quartile representing 25% of the data. At bottom are spike density functions generated by applying a Gaussian kernel (δ = 100 ms) to the corresponding spike trains from A-C. (**D-F**) Fraction of neurons from male (♂) rats with activity significantly modulated by state value, ΣQ (D), and policy value, ΔQ (E), during action planning and action selection, and chosen value (F) during outcome presentation. (**G-I**) Fraction of neurons from female (♀) rats with activity significantly modulated by state value, ΣQ (G), and policy value, ΔQ (H), during action planning and action selection, and chosen value (I) during outcome presentation. In B-I, horizontal dashed lines indicate chance level (binomial test, $\alpha = 0.05$). *$p < 0.05$, ***$p < 0.001$, logistic regression with Generalized Linear Mixed-Effect Model for D-I. n = 247 neurons from 9 air male rats, 504 neurons from 8 EtOH male rats, 347 neurons from 5 air female rats, and 354 neurons from 5 EtOH female rats.

Lastly, we examined how EtOH pre-exposure affects value updating during the outcome feedback period by regressing firing rates aligned with the onset of outcome presentation as linear functions of the action value of the chosen option (chosen value, Qc), while accounting for the effects of choice and outcome in the analysis (**Figures 5C, 5F and 5I**). The impact of EtOH on neural encoding of the chosen value varied depending on sex ($p < 0.0001$. interaction among treatment, sex and time). We found a greater proportion of neurons encoded the chosen value at the beginning of outcome presentation (~0-400 ms) in EtOH male rats than their air controls (**Figure 5F**; $p = 0.017$, interaction between treatment and time). By contrast, the chosen value was

represented in fewer neurons in EtOH female rats than their air controls (**Figure 5I**; p = 0.035, main effect of treatment in female rats).

These results suggest that EtOH differentially alters the neural representation of state values and action policy during the distal action planning phase (i.e., ITI period and trial onset) and the neural representation of value updating of chosen actions during the outcome processing period in males and females, with overall greater impacts on males.

Discussion

In the present study, we demonstrated that chronic EtOH vapor exposure during adulthood induces long-lasting behavioral deficits in rats, which manifest in a sex-specific manner and persist for over 10 weeks after withdrawal. Using behavioral data from the dynaPR task, but not the simple PRL task, it was possible to predict sex and the history of EtOH exposure in male subjects based on their performance. Cycles of high-dose EtOH exposure impaired adaptive learning under conditions of high uncertainty and led to a general tendency to repeat the same choice regardless of outcome in male, but not female, rats. To elucidate mechanisms underlying these behavioral deficits in males, we tested different RL models. Our findings indicate that chronic EtOH exposure increased the reward-mediated learning rate for updating the value of chosen actions in both female and male rats. In male rats, however, this exposure selectively enhanced the forgetting rate when reward is omitted, amplifying the decay of unchosen action values and heightening the weight of chosen actions. Furthermore, EtOH exposure differentially altered the firing patterns of dorsomedial striatum (DMS) neurons in male and female rats. In males, EtOH exposure strengthened the representation of outcome and chosen value, while it diminished responsiveness to choice, policy, and state signals, a pattern of changes that aligns with the reduced cognitive control of action-selection and deficits in outcome-specific value updating observed in EtOH males. Conversely, in females, EtOH exposure specifically enhanced neural encoding related to choice and prolonged the duration of outcome representations, without significantly impacting the encoding of other decision variables. Our findings shed light on the sex-dependent cognitive and neural computational mechanisms underlying drug-induced persistent deficits in cognitive flexibility.

Influences of EtOH exposure history on action strategies and reward learning

Human studies have linked chronic EtOH abuse and withdrawal with long-lasting cognitive impairments (42-44). However, in rodent studies, the evidence for enduring impacts of EtOH on cognitive flexibility has been mixed. Promising results have emerged from reversal tests within attention set-shifting tasks (13, 45) (but see also (46)) and the spatial Barnes maze (47), although findings are less consistent in probabilistic reward reversal tasks (36, 37, 46, 48, 49).

In the present study, we focused on two-choice probabilistic learning procedures, which rely on trial-and-error learning within sessions of hundreds of behavioral trials, and are thus amenable to computational modeling to characterize specific steps in learning processes (50), for identification of cognitive mechanisms that may underlie EtOH-induced deficits. Our findings from a standard probabilistic reversal learning (PRL) task showed no significant behavioral changes after EtOH exposure, consistent with prior studies in both rodents (36, 37) and humans (51). EtOH-naïve rats in the PRL task demonstrated a lower win-stay probability and a lower probability of staying with the preferred option from the previous block compared to the dynaPRL. This indicates that our dynaPRL task, through varying reward probabilities and unpredictable transitions, introduced more uncertainty and required a higher learning rate in rats (32, 38, 52).

With this more challenging dynaPRL task, we uncovered EtOH-induced cognitive deficits that are sex-dependent. When facing sudden cognitive challenge in the dynaPRL task, EtOH males, but not females, exhibited a moderate but reliable deficit in adaptive learning, i.e., a higher probability of repeating their choice, especially after reward omission in a high-uncertainty environment. Additionally, male EtOH rats exhibited less deviation from matching their choices to the inferred reward schedule (53). These findings suggest that EtOH rats, especially males, might favor exploitation over exploration, generally in line with human studies (54). Exploration-exploitation behaviors are modulated by uncertainty and outcome novelty (55).

One plausible explanation for the EtOH-induced reduction in exploration is that chronic EtOH exposure either decreases uncertainty-mediated exploration (56) or promotes uncertainty avoidance following unrewarded choices, independent of learning (55). This may also explain why behavioral deficits with standard PRL, in which the uncertainty levels are lower and constant, have been less frequently observed, whereas our dynaPRL might provide favorable conditions for observing deficits given the greater challenge to animals to adapt their learning process according to changing uncertainty. Indeed, humans with EtOH use disorder display aberrant decision-making amidst high ambiguity in the Iowa Gambling Task (57). The intolerance of uncertainty has also been associated with risky EtOH use behavior (58) and “hyperkatifeia” (59).

Another possible explanation for the reduced exploration behavior is that EtOH pre-exposure may impair the processing of outcomes, thereby diminishing outcome sensitivity and altering decision-making under uncertainty. To estimate outcome learning processes, we used RL, a theoretical framework for describing the cognitive process of value-based decision-making (60) that has been informative for the dissection of pathological decision making in animal models of addiction (61). In males, a history of chronic EtOH exposure enhanced the updating of chosen action value upon receiving rewards, indicating heightened reward sensitivity, and also facilitated the decay of the unchosen action value when unrewarded, reflecting a diminished emphasis on negative feedback on chosen action. These alternations of reward learning in males may emphasize selected actions more regardless of their outcomes, leading to increased likelihood of behavioral exploitation. This result aligns well with RL modeling of behavior of alcohol dependent humans alcohol users (62). Importantly, we observed similar but dramatically weaker trends of changes in outcome processes in females, further suggesting that high behavioral perseveration and exploitation in males stem from hypersensitivity to distinct outcomes. Taken together, our results show that male rats are more susceptible to the negative impacts of chronic EtOH vapor exposure on uncertainty-driven behavioral flexibility than female rats within the dynaPRL task.

Human studies on sex differences in the impact of chronic EtOH on cognitive function have produced mixed results, with some showing greater, lesser, or indistinguishable effects in women compared to men (30, 63-65). The reasons underlying these variations in results are multifaceted and influenced by factors such as the type of cognitive task, age, socioeconomic status, hormonal differences, and drinking pattern (64, 65). Laboratory rodent models provide a setting in which many of these variables are either absent or controlled. One study found chronic intermittent ethanol (CIE) vapor exposure impairs goal-directed decision-making in male rats but not in females (66), in line with findings here. In a study of the impact of prenatal alcohol, males also appear more susceptible to later cognitive deficits than females (67). The sex-specific effects of EtOH observed in the present work may be attributed to several factors. First, we identified sex-based differences in basal cognitive processes, such as choice strategy, in the dynaPRL task. This finding suggests potential sex differences in explore-exploit strategies and motivations, supporting the idea that male and females engaged different cognitive process to learn or perform the task (5,

68). These sex differences in behavior may modulate susceptibility to neuropsychological impairments (69, 70), in that a high exploitation trait may make males more vulnerable to the impact of EtOH on cognitive flexibility. Additionally, inherent sex differences in processing uncertainty, especially under cognitive challenge and stress, could also contribute to these observed behavioral differences (71). It is also possible that neuroprotective factors, such as estrogen, might mitigate EtOH effects in female rats (72).

Sex-specific neural adaptations to EtOH in the dorsomedial striatum

Numerous studies support a critical role for the DMS in encoding decision-related variables (1, 2, 4, 7-9, 23, 41) and controlling action selection in value-based decision tasks (4, 8, 9, 23, 25, 73, 74). The overall pattern of changes in neural encoding of these variables in male rats exposed to EtOH is congruent with the reduced exploration we observed. First, the rapid decay of neural choice signals in EtOH exposed rats during the outcome presentation phase might hamper the temporal credit assignment process (75-77), weakening response-outcome associations. Additionally, the EOH-induced enhancement of outcome encoding in males may lead to the asymmetric facilitation of chosen action value updating observed in our study (**Figure 3**), increasing the learning rate for chosen values and accelerating the decay of unchosen values on trials without reward. In line with the RL modeling results, we observed an enhanced representation of chosen value in the DMS after EtOH exposure, which could lead to an overemphasis on the chosen option over alternatives, resulting in greater behavioral perseveration, reduced exploration, and ultimately, a loss of cognitive flexibility. Finally, the changes in state value encoding also are in-line with the behavioral observations. In the present study, state value indicates the richness of the environment, which is a strong indicator of block type (**Figure S11**). This information can facilitate the construction of a 'world model' to guide action selection or help reduce uncertainty in action selection. Therefore, the rapid decay of state value representation in EtOH-exposed animals during the choice preparatory period might impair the DMS's ability to integrate environmental information, potentially hindering flexible model-based action selection. This reduction of state value signals, alongside the disruption of choice signals, could serve as another parallel mechanism to exacerbate poor response-outcome associations, ultimately causing males to be less exploratory in decision-making.

Female rats, however, displayed a different pattern of neural activity. Their basal neural responses to decision variables differed from males, and chronic EtOH exposure affected their neural encoding in a distinct manner. The dynamics of DMS encoding of choice and outcome during outcome presentation differed in EtOH-exposed females compared to EtOH-naïve females, with a lower representation of chosen value signals compared to their air-treated controls, a pattern opposite to that observed in males. The observed sex differences in DMS sensitivity to EtOH are unlikely to result from basic physiological properties of the recorded cells, since these properties are similar across sexes (78). While estrous cycle can influence female neural physiology (78), sampling across several weeks likely averaged out these cycle-dependent changes in the present study. Despite detection of some EtOH-induced neural encoding differences, surprisingly, we observed no significant EtOH-induced performance differences in females, suggesting that female rats may possess compensatory mechanisms that mitigated the effects of EtOH exposure on neural encoding in the DMS, thereby preserving flexible value-based decision-making. Of course, our EtOH treatment may have induced cognitive alterations in females to which our task was not sensitive. Thus, more research with a broad assortment of cognitive tasks is needed to fully understand the sex-specific neural and behavioral adaptations to drug exposure and to develop female-sensitive tasks that effectively capture these differences.

The striatum is composed of multiple neuronal types. We note that our conclusions remained unchanged even after removing the small proportion of presumed fast-spiking striatal neurons (firing rate >18 Hz) from our datasets. Given that medium spiny neurons are the principal neurons in the rat striatum (> 95%) (79), this suggests that the EtOH-evoked, sex-specific effects are primarily observed in medium spiny neurons, a conclusion that remains to be confirmed in the future with cell type-specific manipulations and measurements.

In summary, this study has unveiled sex-specific and enduring behavioral and neural consequences of chronic EtOH exposure, providing new insights into mechanisms underlying cognitive impairments associated with EtOH addiction. Chronic EtOH exposure persistently and differentially distorts neural computational processes in males and females. Female rats exhibited distinct basal behavioral and neural dynamics during decision making which suggest the engagement of different computational systems that may be differentially impacted by EtOH, thereby avoiding the cognitive inflexibility observed in male rats. These mechanisms identified in males may underlie some of the cognitive deficits observed in humans with alcohol use disorder. Low cognitive flexibility imposes a higher risk of alcohol use disorders (80). Importantly, behavioral and neural mechanisms for the changes we observed here after chronic EtOH might resemble those underlying loss of cognitive flexibility after chronic use of other drugs of abuse (81) or other psychiatric disorders (82).

Materials and Methods

Animals

17 Male and 10 female Long-Evans (LE) wild-type rats (10 wks old upon arrival, Envigo) were singly housed. Rats were kept in a temperature- and humidity-controlled environment with a light:dark cycle of 12:12 h (lights on at 7:00 a.m.). Experiments were conducted during their light cycle. All animal procedures were approved by the Johns Hopkins University Animal Care and Use Committee. The protocol number is RA23A232.

Probabilistic reversal learning (PRL) task

Rats undergoing behavioral testing were water-restricted to 90% of their *ad-libitum* weight. Behavioral experiments were performed in a soundproof customized modular operant chamber (Med Associates). The levers and a reward magazine were confined to the same wall of the chamber. Rats were initially trained to enter the magazine to collect reward by delivering a 100 µl reward (10% w/v sucrose in tap water) at random times with an average interval of 60 s (RT60). Subsequently, rats were trained to initiate a trial by entering the magazine, which triggered insertion of two levers into the chamber. Pressing a lever led to reward delivery (at this stage, both levers provided reward with 100% probability). Next, rats were trained on the reversal task, in which pressing one lever consistently delivered a reward (100% probability) and the other lever was not rewarded (0% probability). These action-outcome contingencies were reversed randomly 8 trials after the value of an exponential moving average over the past 8 choices (1 for correct and 0 for incorrect choice) crossed a 0.75 threshold. The block reversal probability was 10%. If the block was not switched within 20 trials of crossing the threshold, the computer forced the reversal. Thus, each rat had adequate trials to acquire current contingencies and could not predict the contingency reversal. One to three days after the deterministic reward schedule (100% and 0%) training, training in the full PRL task began. The reward probabilities for each lever were selected from 70% and 10%. Each trial in the PRL task began with illumination of the reward magazine. Upon a poke into the magazine (trial initiation), two levers flanking the left and right sides of the port were inserted after a variable delay (randomly selected between 100 ms to 1 s with 100 ms intervals). Rats were given 30-s to press a lever; failure to do so resulted in an invalid trial (<1% of trials for all rats) that was excluded from analysis. A lever press probabilistically resulted in either the CS- (0.5 s of white noise generated by MED Associated, ENV-225SM) with no reward delivery or the CS+ (two clicker sounds with a 0.1-s interval generated by MED Associated, ENV-135M) with ~33µl reward delivery in the magazine via a syringe pump (MED Associated, PHM-100). Each trial ended either at the end of the CS- presentation or after completing the reward collection (exit from the first magazine entry after reward delivery). Trials were separated by a constant 2.5-s intertrial interval (ITI). Each behavioral session lasted ~ two hours. All rats experienced 15 sessions of PRL prior to the vapor procedure and on average ~10.07 sessions of PRL after the vapor procedure.

Chronic intermittent EtOH vapor exposure (CIE)

We counterbalanced rats based on their behavioral performance in the PRL task prior to 4 sessions of habituation to the vapor chambers. After that, rats were exposed to four cycles of EtOH vapor (n = 8 male and 5 female) or air (n = 9 male and 5 female) (14, 35). Each cycle consisted of 14 hrs of vapor exposure followed by a 10-hr withdrawal, repeated for 5 consecutive days. EtOH was volatilized by venting air through a heating flask containing 95% EtOH at a rate of 30-40 l/min. EtOH vapor was delivered to rats housed in Plexiglas chambers (La Jolla Alcohol Research,

inc.). Blood was collected from the tip of tails in the middle and end of each round from all EtOH-exposed rats to assess blood EtOH concentrations (BECs) with an AM1 alcohol analyzer from Analox Inc. To control the stress of the blood collection, we pinched the tip of tails for air control rats instead of cutting the tissue and collecting blood. Our procedure produced a mean BEC of 224.95 ± 14.51 (S.E.M) in male and 257.2 ± 23.79 (S.E.M) mg/dl in female rats without significant sex differences (**Figure 1A**, inset), which is in line with previous findings (14, 35).

Dynamic probabilistic reversal learning (dynaPRL) task

Water-restricted rats performed this task in the same operant chamber as the original PRL task. The task structure was the same as PRL above except that reward probabilities assigned to each lever were drawn pseudorandomly from a set of blocks with paired probabilities [block1(neutral): (0.45, 0.45), block2(low contrast): (0.6, 0.3), block3(high contrast): (0.8, 0.1)] (**Figure 1F**). Note that each block type had a distinct probability contrast (block1, 1:1; block2, 2:1; block3, 8:1), while maintaining the same average reward probability (0.45), and that the outcome uncertainty within a block varied with the degree of probability contrast across the two levers, i.e., high uncertainty in a low contrast block, etc. The lever outcome contingencies were randomly reversed to one of the three blocks every 15-30 trials, except when a rat made four or more consecutive incorrect choices within certain trial blocks (block2: 60,30 or block3: 80,10); such trials were excluded from trial progress. When switching blocks, the transition rules imposed two restrictions: 1) the position of the lever with the highest reward probability should not be the same in two consecutive blocks even if the reward probability contrast changes, and 2) neutral blocks (block1) should not be repeated. Block transitions were categorized into three types based on the relative cognitive challenge level before and after each block transition. If the relative uncertainty was lower in the post-reversal block compared with the pre-reversal block, this was termed a 'Hi-Lo' transition (i.e., block2→block3, block1→block2, or block1→block3). If the relative uncertainty was higher in the post-reversal block compared with the pre-reversal block, this was termed a 'Lo-Hi' transition (i.e., block3→block2, or block2→block1, or block3→block1). If the relatively uncertainly was the same in the post-reversal block compared with the pre-reversal block while still shifting probabilities across the right and left levers, this was termed a 'Same' transition (i.e., block2→block2 or block3→block3). In addition, in this task, during non-neutral blocks (i.e., blocks 1 and 3) in 40% of the trials after the first post-reversal 12 trials, we probed the animal's response to unexpected changes in reward size by doubling or halving the reward size (66 or 16.5 μl) compared to the remaining 60% of the trials. However, EtOH exposure did not alter choice strategy relative to distinct reward sizes; thus, we do not focus on this feature in this report. Rats were trained on the final dynaPRL task for at least 10 sessions prior to surgery.

Electrode implantation

All rats were surgically implanted with custom-made drivable electrode arrays, with custom-designed 3D-printed pieces, sixteen insulated tungsten wires (50 um, A-M Systems), and two silver ground wires, soldered to two Plexon headstage connectors (Plexon Inc. TX) using standard stereotaxic procedures. Electrode arrays were placed unilaterally in the left or right DMS (AP: -0.1 mm; ML: 2.45 mm; DV: -4.7 mm from Bregma).

Recording and Spike sorting

Following 1 week of recovery, rats were trained on the dynaPRL task again until they became accustomed to performing while their headstage was connected via a patch cable to the commutator located in the center of the chamber ceiling. Once their completed trials/session

reached at least 80% of their pre-surgery mean number of trials in a session (3-7 sessions), recording sessions began. Electrical signals and behavioral events were collected using Plexon multichannel neural recording systems (MAP system;) or Plexon OmniPlex systems, with a 40 kHz sampling rate. Neural recordings at the same depth in the DMS were obtained for multiple sessions; if multiple sessions from the exact recording location were included in the following analysis, the data from the same channel was included only once. After that, electrodes were lowered by approximately 160 μm, and recording resumed in the new location at least one day later. When recordings were complete, electrode sites were labeled by passing a DC current (50 μA, 30 s, cathodal) through one channel of each electrode, and recording locations were verified histologically as previously described (83). All subjects were included after verification of electrodes placement.

Individual units were isolated offline using principal component analysis in Offline Sorter (Plexon) as described previously (83). Auto-correlograms, cross-correlograms, the distribution of inter-spike intervals, L-ratio, and isolation distance were used to ensure good isolation of single units. Spike and behavioral event timestamps were exported to MATLAB (MathWorks) using customized scripts for further analysis. Recorded units were classified based on firing rate and waveform width; however, no clear clustering patterns emerged (**Figure S8D**). Most neurons (>90%) had firing rates below 18 Hz (**Figure S8E**), likely representing putative medium spiny neurons (MSNs), with this proportion aligning with the typical composition of neurons in the rat striatum (79). Because we were interested in encoding of behavioral variables by the full DMS population we included all units in our analyses. However, analyzing only lower firing units resulted in identification of highly similar population-level encoding.

Data Analysis and Statistics

Sessions with a minimum of 150 trials were included in the subsequent analyses.

Behavioral metrics

Reversal performance

Reversal performance was assessed by the probability of maintaining the same choice before the contingency change, denoted as *p(perseveration)*. *p(perseveration)* was computed for each trial during the last 5 trials before and the first 12 trials after the contingency change by the ratio of correct choices and the total number of blocks, except that if the pre-reversal block was a neutral block, in which neither side is correct, then a random side was selected as a pseudo-correct choice for the calculation. A single exponential decay function was fit to the p(preservation) for 1-12 trials after the contingency change,

$$p = d + a \times e\text{^}(-\lambda \times t) \qquad (1)$$

where d, a, and λ represent the pre-reversal asymptotic value, the magnitude of change in *p(perseveration)* after the reversal, and the learning speed, respectively. The single exponential decay function was defined by MATLAB function *fittype* and curve fitting employed MATLAB function *fit* with lower boundary (0, 0.5, 0) and upper boundary (3, 2, 1) for parameters d, a, and λ correspondingly. Averaged parameter values across 9 iterations were used for each subject and session.

Matching performance, stay probabilities, and latencies

To assess how animals allocate their responses (left and right lever presses) to the local (within a block) reward probabilities of each choice option after the learning period (first 12 trials), we

calculated the *matching score* (40) as a deviation of left response probability, *p(left)*, from the reward probability given selection of the left choice, *p(reward|choice=left)*. Deviation < 0 is undermatching, and > 0 is overmatching.

We measured the overall stay probability by calculating the likelihood of repeating the same choice as the last trial. Conditional stay probabilities were calculated separately for the reward or unrewarded outcome in the last trial and denoted as *p(stay|win)* and *p(stay|lose)* correspondingly. The difference between win-stay and lose-shift (ΔWSLS) was obtained by the difference between *p(stay|win)* and *p(shift|lose)*. The analysis here was reused code from the following link: *https://github.com/DartmouthCCNL/trepka_etal_natcomm_2021*.

The latencies (response times) measured included the time interval between stimulus (center light illumination or lever insertion) and response or reaction (magazine entry or lever press) to that stimulus. As the distribution of latencies is highly skewed to the left (zero), a natural logarithm transformation was used to make the distributions of latencies more akin to normal distributions.

Classification analysis

Support vector machine (SVM)

An SVM was employed to decode group membership (CIE vs. Air), sex label (male vs. female), and assessment phase (only for PRL task, pre-vapor vs. post-vapor) from the behavior dataset (**Figure S2A**). SVM modeling was performed using the MATLAB function *fitclinear* for the classification of binary group membership and *fitecoc* for the classification of multi-subject labels. For both classification approaches, we used a total of 20 behavioral measures (columns) from each session (**Table S1**).

The behavior dataset was randomly divided into two parts, a training set and a test set with a 90:10 ratio. Within the training set, a linear SVM model was optimized using 10-fold cross-validation. This approach involves dividing the training set into 10 equal parts, training the model on nine parts, and validating it on the tenth part. This process is repeated ten times, with each part used once as the validation set. The results from these iterations are used to fine-tune the model parameters. The optimized SVM model was then evaluated on a test set to assess its generalizability and predictive performance. This train-test process was repeated 1000 times. True positive (TP), true negative (TN), false positive (FP, type I error), and false negative (FN, type II error) were calculated based on actual predicted data labels. For the multilabel classification, precision [TP/(TP+FP)] was used to assess model performance in predicting each class. To determine whether the observed decoding accuracy for group membership and sex label was significantly higher than what would be expected by chance, we conducted Monte Carlo significance tests, and the p-value was computed as follows:

$$p = \frac{NP + 1}{N + 1} \tag{2}$$

Here, *NP* is the number of iterations where the decoding precision of an SVM model trained with a shuffled dataset is higher than that of the observed dataset [precision (Shuffle) > precision (Data)] and *N* is the number of all iterations.

To assess the contribution of individual behavioral features to the classification of sex labels in EtOH-naïve control rats, we employed the feature selection method of maximum relevance and minimum redundancy (fMRMR) using MATLAB. We directly applied the fMRMR function to

the behavioral dataset, which was previously used to train the SVM classifier. This method allowed us to identify the most relevant features for distinguishing between male and female labels while minimizing redundancy among them. The importance score for each feature was defined based on its relevance to the classification task and its redundancy with other features, providing insights into the key behavioral features contributing to the classification.

Uniform manifold approximation and projection (UMAP)

The manifold learning technique, UMAP, was employed to perform non-linear dimensional reduction of our behavior data matrix from above. We used the UMAP implementation provided in the MATLAB community *UMAP*, which is available via the following link: *https://www.mathworks.com/matlabcentral/fileexchange/71902-uniform-manifold-approximation-and-projection-umap*.

Reinforcement learning models

Reinforcement learning (RL) models assume that choices stem from the cumulative outcomes of actions accrued over numerous trials. We fitted the choice and outcome data to eight distinct RL models: 1, standard Q-learning model; 2, Q-learning model with differential learning rates (Q-DFLr); 3, differential forgetting RL model (DF-RL); 4, DF-RL model with inverse temperature β (DF-RLwβ); 5, forgetting RL model (F-RL); 6, F-RL model with inverse temperature β (F-RLwβ); 7, win-stay lose-shift model (WSLS); 8, biased random choice model (RD).

For models 1 through 4, choices are assumed to follow learned values for each option, Q, according to softmax function, in which the probability of choice *k* on trial *t* is:

$$P_k(t) = \frac{e^{\beta Q_k(t)}}{\sum_{i=1}^{k} e^{\beta Q_k(t)}} \tag{3}$$

Here, β is the inverse temperature parameter that controls the level of stochasticity in the choice, with β = 0 resulting in equal probability over all choice options. β was set to a constant 1 for models 4 and 6.

The value updating for each model is described below:

Model 1: Q-learning model,

If $c(t)$ = L,

$$Q_L(t+1) = Q_L(t) + \alpha\big(\mathrm{r(t)} - Q_L(t)\big) \tag{4}$$

$$Q_R(t+1) = Q_R(t) \tag{5}$$

where $c(t)$ is the choice side (left, L or right, R) in the current trial, $r(t)$ is the outcome on that trial, and α is the learning rate, controls the update of the chosen action value according to the reward prediction error $r(t) - Q_L(t)$.

Model 2: Q-learning model with differential learning rates (Q-DFLr),

If $c(t)$ = L and $r(t)$ = 1,

$$Q_L(t+1) = Q_L(t) + \alpha^{+}\big(\mathrm{r(t)} - Q_L(t)\big) \tag{6}$$

$$Q_R(t+1) = (1 - \theta^{+})\, Q_R(t) \tag{7}$$

If $c(t)$ = L and $r(t)$ = 0,

$$Q_L(t+1) = Q_L(t) + \alpha^{-}\big(\mathrm{r(t)} - Q_L(t)\big) \tag{8}$$

$$Q_R(t+1) = (1 - \theta^{-})\, Q_R(t) \tag{9}$$

Here, value updates are governed by different learning rates for positive, α^{+}, or omitted, α^{-}, outcomes and the non-chosen option is decay by a forgetting rate, θ^{+} or θ^{-}, for rewarded and unrewarded trials respectively.

Model 3 and 4: Differential forgetting RL (DF-RL) and DF-RL with (model 4) or without (model 3) free β,

If $c(t)$ = L and $r(t)$ = 1,

$$Q_L(t+1) = \gamma_c Q_L(t) + k^{+} \tag{10}$$

$$Q_R(t+1) = \gamma_{uc} Q_R(t) \tag{11}$$

If $c(t)$ = L and $r(t)$ = 0,

$$Q_L(t+1) = \gamma_c Q_L(t) + k^{-} \tag{12}$$

$$Q_R(t+1) = \gamma_{uc} Q_R(t) \tag{13}$$

where κ^{+} and κ^{-} directly update the chosen action value in rewarded and unrewarded trials, respectively. γ_c and γ_{uc} are the forgetting factor in updating chosen and unchosen action values, respectively. Accordingly, forgetting rates θ_c and θ_{uc} in models 3 and 4 correspond to 1-γ_c and 1-γ_{uc}, respectively.

Model 5 and 6: Forgetting RL models (F-RL) and F-RL with (model 6) or without (model 5) free β,

If $c(t)$ = L and $r(t)$ = 1,

$$Q_L(t+1) = \gamma Q_L(t) + k^{+} \tag{14}$$

If $c(t)$ = L and $r(t)$ = 0,

$$Q_L(t+1) = \gamma Q_L(t) + k^{-} \tag{15}$$

For the unchosen right side,

$$Q_R(t+1) = \gamma Q_R(t) \tag{16}$$

where κ^{+} and κ^{-} directly update the chosen action value in rewarded and unrewarded trials, respectively. γ is the forgetting factor in updating chosen and unchosen action values.

Models 7 and 8 directly describe the probability of each choice option on trial t, either subject to experienced outcomes (WSLS) or as a fixed proportion of choice.

Model 7: Win-stay lose-shift.

If $c(t)$ = L and $r(t)$ = 1,

$$P_L(t+1) = 1 - \epsilon/2 \tag{17}$$

$$P_R(t+1) = \epsilon/2 \tag{18}$$

If $c(t)$ = L and $r(t)$ = 0,

$$P_L(t+1) = \epsilon/2 \tag{19}$$

$$P_R(t+1) = 1 - \epsilon/2 \tag{20}$$

Where ϵ controls the randomness of the stay probability.

Model 8: Biased random choice.

$$P_L(t+1) = \varphi \tag{21}$$

$$P_R(t+1) = 1 - \varphi \tag{22}$$

Where φ controls the bias of choice probability.

Hierarchical model fitting and model comparisons

We used the Matlab Stan interface (https://mc-stan.org/users/interfaces/matlab-stan) to construct and sample from hierarchical RL models, in which group-level hyperparameters govern individual rat parameters, to avoid overfitting to inter-rat noise. For a given model, we used Stan to draw consecutive samples from the posterior density of the model parameters using Hamiltonian Markov chain Monte Carlo (HMC), giving density estimates for the best fitting model parameters for the aggregate choice and outcome data across all sessions and rats. For each model, rat-level parameters were drawn from a group-level distribution with group mean, μ, group mean difference, δ, and variance σ. To quantify the evidence of group differences, the Directed Bayes Factor (dBF) was employed. This measure calculates the ratio of the proportion of the distribution of δ (group difference) that is above zero to the proportion that is below zero as in (84). Given the difficulties in sampling from hierarchical RL models, parameters were transformed such that sample were drawn in an unconstrained space and later transformed into bounded values using the fast approximation of the cumulative normal distribution function, *phi_approx*. We set normally distributed priors for all parameters at the rat level: N(0, 1) for all parameters, except β, which was set at N(0, 10), while group-level hyperparameters were given a prior normal prior distribution of N(0, 2) for μ and δ; and a gamma distribution of (2, 0.5) for σ. Hierarchical models for each of the candidate RL models were sampled for 2,000 iterations after 1,000 warm-up draws for four chains in parallel. All other settings adhered to the default configuration.

Predictive accuracy of each model was estimated using leave-one-out cross validation with Pareto-smoothed importance sampling (psis-loo) using the model log likelihood computed for each of the sampled parameters on the actual choice and outcome data. For simulations of behavior, we took the mean of the posterior samples (i.e. over the 2000 post-warm up draws) for each rat-level model parameter as the best-fitting estimate for that individual subject. Using these best-fitting model parameters, we simulated choice behavior on the actual task structure. A reversal analysis, analogous to the one used on the empirical data, was applied to these simulated data to probe whether the model could recapitulate the key differences in choice behavior observed in the empirical data.

Multiple linear regression

To examine how neural spike activity was modulated by different behavioral and decision variables, we employed multiple linear regression models to fit spike rates of each unit as a linear function of various factors, such as rat's choice, reward outcome, and estimated action values as in (2, 41). All trials in each session other than those with choice omission were included in the analysis. The number of trials was matched across groups (**Figure S8F**). To investigate the evolution of neural spike modulation within a temporal window surrounding key behavioral events, including lever insertion, action selection, and outcome presentation, we aligned the spikes of each

neuron to the onset of these behavioral events. We then quantified the firing rates of each neuron using a sliding time bin approach. Specifically, we employed a 100-ms time bin with 50-ms steps or a 200-ms time bin with 100-ms steps. This analysis was conducted within predefined temporal windows relative to trial onset, trial initiation, lever insertion, lever press, and outcome, presentation, which were set at -2300 ms to 600 ms, -700 ms to 300 ms, -500 ms to 500 ms, -500 ms to 500 ms, and -100 ms to 1000 ms, respectively. To control for the temporal auto-correlation among spikes, we added auto-regression (AR) terms as in Shin et al. (41) for all of the following regression models. To investigate the influence of both current and preceding choices, outcomes, and their interaction on the spike activity of individual neurons, we employed a regression model to delineate the firing rate (*S*) as a function of choice direction (*C*; ipsi or contra-lateral to implant side), outcome (*O*; rewarded or unrewarded), and their interaction (*I*) in current trial *t* and last trial *t*-1, along with autoregressive components (*AR*), as the following

$$S(t) = \beta_0 + \beta_1 \times C(t) + \beta_2 \times C(t-1) \; + \; \beta_3 \times O(t) + \beta_4 \times O(t-1) \\ + \; \beta_5 \times I(t) + \beta_6 \times I(t-1) \; + \; AR \; + \varepsilon(t) \tag{23}$$

where β_0 through β_6 represent standardized regression coefficients, and the error term is $\epsilon(t)$. AR term was defined as follows:

$$AR \; = \; \beta_7 \times S(t-1) \; + \; \beta_8 \times S(t-2) + \beta_9 \times S(t-3) \tag{24}$$

To examine how chosen value-related signals are represented by neurons at the time that choice and outcome are revealed, we used the following regression:

$$S(t) = \beta_0 + \; \beta_1 \times C(t) + \beta_2 \times O(t) + \; \beta_3 \times I(t) \\ + \beta_4 \times Q_c(t) + AR \; + \varepsilon(t) \tag{25}$$

where Q_c is the chosen value estimated by the best fit RL model.

To investigate how different types of value signals are encoded in neuronal activity, we used a regression model as follows:

$$S(t) = \beta_0 + \; \beta_1 \times C(t) + \beta_2 \times \Sigma Q(t) + \; \beta_3 \times \Delta Q(t) \\ + \; \beta_4 \times Q_c(t) + AR \; + \varepsilon(t) \tag{26}$$

Where ΣQ is the summation of action values of ipsilateral (Q_{ipsi}) and contralateral choice (Q_{contra}) and ΔQ is the difference between Q_{ipsi} and Q_{contra}, which can approximate state value and policy, respectively (2, 41).

Generalized linear mixed-effect models (GLMMs)

To understand the impact of EtOH treatment, sex and time during the epoch on the proportion of neural responses to specific decision variables described above, we employed a Generalized Linear Mixed-Effects Model (GLMM) to account for the random effects associated with individual animals and specific neurons within those animals. The model is described by the following Wikison notation:

$$RS \sim Group * sex * \; bin + (1|RatID) + (1|RatID{:}\,NeuronID) \tag{27}$$

Where *RS* denotes significance of response, a binary variable indicating whether the response is modulated significantly, as determined by the preceding multiple linear regression. The fixed effects in the model include *Group* (representing the experimental conditions, such as EtOH or

Air), *bin* (representing time bins of spike activity), and the interaction term *Group:bin* (representing the interaction between the experimental conditions and time bins). *RatID* and *NeuronID* are random effects. The term "*1|RatID*" introduces a random intercept for each animal, allowing for the acknowledgment of variability in baseline response levels across animals. The term "*1|RatID:NeuronID*" adds another layer of random intercepts, this time to account for variability at the neuron level within each animal, acknowledging that responses may differ not just between animals but also among neurons within the same animal. If a sex-dependent interaction was observed, we conducted additional GLMM analyses within each sex as a post-hoc test, using the following Wilkison notation

$$RS \sim Group * bin + (1|RatID) + (1|RatID{:}NeuronID) \tag{28}$$

To fit this model, we utilize the *fitglme* function in MATLAB with a 'Binomial' distribution and a 'Logit' link function.

Other statistical analysis

Behavioral data with normal distribution or relatively small sample size were analyzed using paired t-tests, one-way ANOVA with repeated measures (one-way RM ANOVA), or mixed effect ANOVA (also known as two-way ANOVA with repeated measures, two-way RM ANOVA) followed by Bonferroni post hoc test. Non-parametric Wilcoxon tests were employed when indicated by non-normal distribution of the behavioral data. Despite potential deviations from normality, a mixed-effect ANOVA (considering both within-sample and between-sample effects) was applied to some behavioral data, given the method's robustness against such violations. The comparison of electrophysiological data encoding distinct properties, characterized by a hierarchical structure with varying numbers of neurons per animal, were analyzed using Generalized Linear Mixed Models (GLMMs) to account for variability at the animal and neuron levels. Additionally, to determine the chance level for the proportion of neurons significantly modulated by decision variables, a binomial test with $\alpha = 0.05$ was conducted. All conducted in MATLAB. A p-value < 0.05 was used as the criterion to determine statistical significance unless noted otherwise. Data analyzed using parametric tests are expressed as the mean ± standard error of the mean (SEM). For data analyzed with non-parametric tests, we present the median, with the interquartile range (IQR) represented by the 1st (25th percentile) and 3rd quartiles (75th percentile). The whiskers on the box plot indicate the range of the data within 1.5 times the IQR from the quartiles, providing a clear visualization of the data distribution and variability.

References

1. M. Ito, K. Doya, Validation of decision-making models and analysis of decision variables in the rat basal ganglia. *J Neurosci* **29**, 9861-9874 (2009).
2. H. Kim, J. H. Sul, N. Huh, D. Lee, M. W. Jung, Role of striatum in updating values of chosen actions. *J Neurosci* **29**, 14701-14712 (2009).
3. B. Lau, P. W. Glimcher, Value representations in the primate striatum during matching behavior. *Neuron* **58**, 451-463 (2008).
4. A. Y. Wang, K. Miura, N. Uchida, The dorsomedial striatum encodes net expected return, critical for energizing performance vigor. *Nat Neurosci* **16**, 639-647 (2013).
5. J. Cox, A. R. Minerva, W. T. Fleming, C. A. Zimmerman, C. Hayes, S. Zorowitz, A. Bandi, S. Ornelas, B. McMannon, N. F. Parker, I. B. Witten, A neural substrate of sex-dependent modulation of motivation. *Nat Neurosci* **26**, 274-284 (2023).
6. A. C. Burton, G. B. Bissonette, N. T. Lichtenberg, V. Kashtelyan, M. R. Roesch, Ventral striatum lesions enhance stimulus and response encoding in dorsal striatum. *Biol Psychiatry* **75**, 132-139 (2014).
7. E. Y. Kimchi, M. Laubach, Dynamic encoding of action selection by the medial striatum. *J Neurosci* **29**, 3148-3159 (2009).
8. S. Nonomura, K. Nishizawa, Y. Sakai, Y. Kawaguchi, S. Kato, M. Uchigashima, M. Watanabe, K. Yamanaka, K. Enomoto, S. Chiken, H. Sano, S. Soma, J. Yoshida, K. Samejima, M. Ogawa, K. Kobayashi, A. Nambu, Y. Isomura, M. Kimura, Monitoring and updating of action selection for goal-directed behavior through the striatal direct and indirect pathways. *Neuron* **99**, 1302-1314 e1305 (2018).
9. D. Lee, H. Seo, M. W. Jung, Neural basis of reinforcement learning and decision making. *Annu Rev Neurosci* **35**, 287-308 (2012).
10. B. J. Mason, Emerging pharmacotherapies for alcohol use disorder. *Neuropharmacology* **122**, 244-253 (2017).
11. V. Manning, S. Wanigaratne, D. Best, R. G. Hill, L. J. Reed, D. Ball, J. Marshall, M. Gossop, J. Strang, Changes in neuropsychological functioning during alcohol detoxification. *Eur Addict Res* **14**, 226-233 (2008).
12. S. Loeber, T. Duka, H. Welzel Marquez, H. Nakovics, A. Heinz, K. Mann, H. Flor, Effects of repeated withdrawal from alcohol on recovery of cognitive impairment under abstinence and rate of relapse. *Alcohol Alcohol* **45**, 541-547 (2010).
13. M. W. Meinhardt, S. Pfarr, G. Fouquet, C. Rohleder, M. L. Meinhardt, J. Barroso-Flores, R. Hoffmann, J. Jeanblanc, E. Paul, K. Wagner, A. C. Hansson, G. Kohr, N. Meier, O. von Bohlen Und Halbach, R. L. Bell, H. Endepols, B. Neumaier, K. Schonig, D. Bartsch, M. Naassila, R. Spanagel, W. H. Sommer, Psilocybin targets a common molecular mechanism for cognitive impairment and increased craving in alcoholism. *Sci Adv* **7**, eabh2399 (2021).
14. R. Renteria, E. T. Baltz, C. M. Gremel, Chronic alcohol exposure disrupts top-down control over basal ganglia action selection to produce habits. *Nat Commun* **9**, 211 (2018).
15. L. H. Corbit, H. Nie, P. H. Janak, Habitual alcohol seeking: time course and the contribution of subregions of the dorsal striatum. *Biol Psychiatry* **72**, 389-395 (2012).
16. G. Dominguez, C. Belzung, C. Pierard, V. David, N. Henkous, L. Decorte, N. Mons, D. Beracochea, Alcohol withdrawal induces long-lasting spatial working memory impairments: relationship with changes in corticosterone response in the prefrontal cortex. *Addict Biol* **22**, 898-910 (2017).

17. Y. Ehinger, Z. Zhang, K. Phamluong, D. Soneja, K. M. Shokat, D. Ron, Brain-specific inhibition of mTORC1 eliminates side effects resulting from mTORC1 blockade in the periphery and reduces alcohol intake in mice. *Nat Commun* **12**, 4407 (2021).
18. Y. Cheng, C. C. Y. Huang, T. Ma, X. Wei, X. Wang, J. Lu, J. Wang, Distinct synaptic strengthening of the striatal direct and indirect pathways drives alcohol consumption. *Biol Psychiatry* **81**, 918-929 (2017).
19. Y. Cheng, X. Xie, J. Lu, H. Gangal, W. Wang, S. Melo, X. Wang, J. Jerger, K. Woodson, E. Garr, Y. Huang, P. Janak, J. Wang, Optogenetic induction of orbitostriatal long-term potentiation in the dorsomedial striatum elicits a persistent reduction of alcohol-seeking behavior in rats. *Neuropharmacology* **191**, 108560 (2021).
20. T. Ma, Y. Cheng, E. Roltsch Hellard, X. Wang, J. Lu, X. Gao, C. C. Y. Huang, X. Y. Wei, J. Y. Ji, J. Wang, Bidirectional and long-lasting control of alcohol-seeking behavior by corticostriatal LTP and LTD. *Nat Neurosci* **21**, 373-383 (2018).
21. B. Bloem, R. Huda, K. I. Amemori, A. S. Abate, G. Krishna, A. L. Wilson, C. W. Carter, M. Sur, A. M. Graybiel, Multiplexed action-outcome representation by striatal striosome-matrix compartments detected with a mouse cost-benefit foraging task. *Nat Commun* **13**, 1541 (2022).
22. F. Gore, M. Hernandez, C. Ramakrishnan, A. K. Crow, R. C. Malenka, K. Deisseroth, Orbitofrontal cortex control of striatum leads economic decision-making. *Nat Neurosci* **26**, 1566-1574 (2023).
23. K. Samejima, Y. Ueda, K. Doya, M. Kimura, Representation of action-specific reward values in the striatum. *Science* **310**, 1337-1340 (2005).
24. L. H. Corbit, P. H. Janak, Posterior dorsomedial striatum is critical for both selective instrumental and Pavlovian reward learning. *The European journal of neuroscience* **31**, 1312-1321 (2010).
25. S. S. Bolkan, I. R. Stone, L. Pinto, Z. C. Ashwood, J. M. Iravedra Garcia, A. L. Herman, P. Singh, A. Bandi, J. Cox, C. A. Zimmerman, J. R. Cho, B. Engelhard, J. W. Pillow, I. B. Witten, Opponent control of behavior by dorsomedial striatal pathways depends on task demands and internal state. *Nat Neurosci* **25**, 345-357 (2022).
26. H. H. Yin, S. B. Ostlund, B. J. Knowlton, B. W. Balleine, The role of the dorsomedial striatum in instrumental conditioning. *The European journal of neuroscience* **22**, 513-523 (2005).
27. R. M. Shansky, Behavioral neuroscience's inevitable SABV growing pains. *Trends Neurosci* **47**, 669-676 (2024).
28. A. K. Radke, E. A. Sneddon, R. M. Frasier, F. W. Hopf, Recent perspectives on sex differences in compulsion-like and binge alcohol drinking. *Int J Mol Sci* **22**, 3788 (2021).
29. A. Flores-Bonilla, H. N. Richardson, Sex differences in the neurobiology of alcohol use disorder. *Alcohol Res* **40**, 04 (2020).
30. N. L. Zabik, J. U. Blackford, Sex and sobriety: Human brain structure and function in AUD abstinence. *Alcohol* **121**, 33-44 (2024).
31. R. van den Bos, J. Homberg, L. de Visser, A critical review of sex differences in decision-making tasks: focus on the Iowa Gambling Task. *Behav Brain Res* **238**, 95-108 (2013).
32. A. Soltani, A. Izquierdo, Adaptive learning under expected and unexpected uncertainty. *Nat Rev Neurosci* **20**, 635-644 (2019).
33. I. E. Monosov, How outcome uncertainty mediates attention, learning, and decision-making. *Trends Neurosci* **43**, 795-809 (2020).

34. D. R. Bach, O. Hulme, W. D. Penny, R. J. Dolan, The known unknowns: neural representation of second-order uncertainty, and ambiguity. *J Neurosci* **31**, 4811-4820 (2011).
35. N. W. Gilpin, A. D. Smith, M. Cole, F. Weiss, G. F. Koob, H. N. Richardson, Operant behavior and alcohol levels in blood and brain of alcohol-dependent rats. *Alcohol Clin Exp Res* **33**, 2113-2123 (2009).
36. C. L. Pickens, M. Gallo, H. Fisher, A. Pajser, M. H. Ray, Alcohol consumption during adulthood does not impair later Go/No-Go reversal learning in male rats. *NeuroSci* **2**, 166-176 (2021).
37. C. G. Aguirre, A. Stolyarova, K. Das, S. Kolli, V. Marty, L. Ray, I. Spigelman, A. Izquierdo, Sex-dependent effects of chronic intermittent voluntary alcohol consumption on attentional, not motivational, measures during probabilistic learning and reversal. *PLoS One* **15**, e0234729 (2020).
38. C. D. Grossman, B. A. Bari, J. Y. Cohen, Serotonin neurons modulate learning rate through uncertainty. *Curr Biol* **32**, 586-599 e587 (2022).
39. A. Funamizu, M. Ito, K. Doya, R. Kanzaki, H. Takahashi, Uncertainty in action-value estimation affects both action choice and learning rate of the choice behaviors of rats. *The European journal of neuroscience* **35**, 1180-1189 (2012).
40. E. Trepka, M. Spitmaan, B. A. Bari, V. D. Costa, J. Y. Cohen, A. Soltani, Entropy-based metrics for predicting choice behavior based on local response to reward. *Nat Commun* **12**, 6567 (2021).
41. E. J. Shin, Y. Jang, S. Kim, H. Kim, X. Cai, H. Lee, J. H. Sul, S. H. Lee, Y. Chung, D. Lee, M. W. Jung, Robust and distributed neural representation of action values. *Elife* **10**, e53045 (2021).
42. S. Chanraud, M. Reynaud, M. Wessa, J. Penttila, N. Kostogianni, A. Cachia, E. Artiges, F. Delain, M. Perrin, H. J. Aubin, Y. Cointepas, C. Martelli, J. L. Martinot, Diffusion tensor tractography in mesencephalic bundles: relation to mental flexibility in detoxified alcohol-dependent subjects. *Neuropsychopharmacology* **34**, 1223-1232 (2009).
43. L. D. Vanes, R. J. van Holst, J. M. Jansen, W. van den Brink, J. Oosterlaan, A. E. Goudriaan, Contingency learning in alcohol dependence and pathological gambling: learning and unlearning reward contingencies. *Alcohol Clin Exp Res* **38**, 1602-1610 (2014).
44. D. Jokisch, P. Roser, G. Juckel, I. Daum, C. Bellebaum, Impairments in learning by monetary rewards and alcohol-associated rewards in detoxified alcoholic patients. *Alcohol Clin Exp Res* **38**, 1947-1954 (2014).
45. S. Kroener, P. J. Mulholland, N. N. New, J. T. Gass, H. C. Becker, L. J. Chandler, Chronic alcohol exposure alters behavioral and synaptic plasticity of the rodent prefrontal cortex. *PLoS One* **7**, e37541 (2012).
46. K. A. Badanich, H. C. Becker, J. J. Woodward, Effects of chronic intermittent ethanol exposure on orbitofrontal and medial prefrontal cortex-dependent behaviors in mice. *Behav Neurosci* **125**, 879-891 (2011).
47. A. Kuzmin, S. Liljequist, J. Meis, V. Chefer, T. Shippenberg, G. Bakalkin, Repeated moderate-dose ethanol bouts impair cognitive function in Wistar rats. *Addict Biol* **17**, 132-140 (2012).
48. C. A. Dannenhoffer, M. M. Robertson, V. A. Macht, S. M. Mooney, C. A. Boettiger, D. L. Robinson, Chronic alcohol exposure during critical developmental periods differentially

impacts persistence of deficits in cognitive flexibility and related circuitry. *Int Rev Neurobiol* **160**, 117-173 (2021).

49. M. H. Ray, T. Hite, M. Gallo, C. L. Pickens, Operant over-responding is more sensitive than reversal learning for revealing behavioral changes after withdrawal from alcohol consumption. *Physiol Behav* **196**, 176-184 (2018).
50. A. Izquierdo, J. L. Brigman, A. K. Radke, P. H. Rudebeck, A. Holmes, The neural basis of reversal learning: An updated perspective. *Neuroscience* **345**, 12-26 (2017).
51. B. Bagci, S. Dusmez, N. Zorlu, G. Bahtiyar, S. Isikli, A. Bayrakci, A. Heinz, D. J. Schad, M. Sebold, Computational analysis of probabilistic reversal learning deficits in male subjects with alcohol use disorder. *Front Psychiatry* **13**, 960238 (2022).
52. J. T. McGuire, M. R. Nassar, J. I. Gold, J. W. Kable, Functionally dissociable influences on learning rate in a dynamic environment. *Neuron* **84**, 870-881 (2014).
53. K. Iigaya, Y. Ahmadian, L. P. Sugrue, G. S. Corrado, Y. Loewenstein, W. T. Newsome, S. Fusi, Deviation from the matching law reflects an optimal strategy involving learning over multiple timescales. *Nat Commun* **10**, 1466 (2019).
54. L. S. Morris, K. Baek, P. Kundu, N. A. Harrison, M. J. Frank, V. Voon, Biases in the explore-exploit tradeoff in addictions: The role of avoidance of uncertainty. *Neuropsychopharmacology* **41**, 940-948 (2016).
55. J. Cockburn, V. Man, W. A. Cunningham, J. P. O'Doherty, Novelty and uncertainty regulate the balance between exploration and exploitation through distinct mechanisms in the human brain. *Neuron* **110**, 2691-2702 e2698 (2022).
56. S. J. Gershman, Uncertainty and Exploration. *Decision (Wash D C)* **6**, 277-286 (2019).
57. A. E. Goudriaan, J. Oosterlaan, E. de Beurs, W. van den Brink, Decision making in pathological gambling: a comparison between pathological gamblers, alcohol dependents, persons with Tourette syndrome, and normal controls. *Brain Res Cogn Brain Res* **23**, 137-151 (2005).
58. M. E. Oglesby, B. J. Albanese, J. Chavarria, N. B. Schmidt, Intolerance of Uncertainty in Relation to Motives for Alcohol Use. *Cognitive Therapy and Research* **39**, 356-365 (2014).
59. G. F. Koob, P. Powell, A. White, Addiction as a coping response: Hyperkatifeia, deaths of despair, and COVID-19. *Am J Psychiatry* **177**, 1031-1037 (2020).
60. N. D. Daw, Y. Niv, P. Dayan, "Actions, policies, values and the basal ganglia" (9, 2006).
61. S. M. Groman, S. L. Thompson, D. Lee, J. R. Taylor, Reinforcement learning detuned in addiction: integrative and translational approaches. *Trends Neurosci* **45**, 96-105 (2022).
62. S. B. Beylergil, A. Beck, L. Deserno, R. C. Lorenz, M. A. Rapp, F. Schlagenhauf, A. Heinz, K. Obermayer, Dorsolateral prefrontal cortex contributes to the impaired behavioral adaptation in alcohol dependence. *Neuroimage Clin* **15**, 80-94 (2017).
63. S. J. Nixon, R. Prather, B. Lewis, "Chapter 16 - Sex differences in alcohol-related neurobehavioral consequences" in *Handbook of Clinical Neurology,* E. V. Sullivan, A. Pfefferbaum, Eds. (Elsevier, 2014), vol. 125, pp. 253-272.
64. R. Fama, A. P. Le Berre, E. V. Sullivan, Alcohol's unique effects on cognition in women: A 2020 (Re)view to envision future research and treatment. *Alcohol Res* **40**, 03 (2020).
65. J. F. Van den Berg, B. Dogge, N. Kist, R. M. Kok, K. Van der Hiele, Gender differences in cognitive functioning in older alcohol-dependent patients. *Subst Use Misuse* **52**, 574-580 (2017).

66. J. M. Barker, K. G. Bryant, J. I. Osborne, L. J. Chandler, Age and sex interact to mediate the effects of intermittent, high-dose ethanol exposure on behavioral flexibility. *Front Pharmacol* **8**, 450 (2017).
67. J. Chandrasekaran, B. Jacquez, J. Wilson, J. L. Brigman, Reinforcer value moderates the effects of prenatal alcohol exposure on learning and reversal. *Front Neurosci* **17**, 1147536 (2023).
68. C. S. Chen, E. Knep, A. Han, R. B. Ebitz, N. M. Grissom, Sex differences in learning from exploration. *Elife* **10**, e69748 (2021).
69. J. D. Salamone, I. Koychev, M. Correa, P. McGuire, Neurobiological basis of motivational deficits in psychopathology. *Eur Neuropsychopharmacol* **25**, 1225-1238 (2015).
70. J. D. Salamone, M. Correa, The mysterious motivational functions of mesolimbic dopamine. *Neuron* **76**, 470-485 (2012).
71. H. Lei, Y. Mochizuki, C. Chen, K. Hagiwara, M. Hirotsu, T. Matsubara, S. Nakagawa, Sex difference in the weighting of expected uncertainty under chronic stress. *Sci Rep* **11**, 8700 (2021).
72. M. E. Jung, M. B. Gatch, J. W. Simpkins, Estrogen neuroprotection against the neurotoxic effects of ethanol withdrawal: potential mechanisms. *Exp Biol Med (Maywood)* **230**, 8-22 (2005).
73. L. H. Tai, A. M. Lee, N. Benavidez, A. Bonci, L. Wilbrecht, Transient stimulation of distinct subpopulations of striatal neurons mimics changes in action value. *Nat Neurosci* **15**, 1281-1289 (2012).
74. J. Lee, B. L. Sabatini, Striatal indirect pathway mediates exploration via collicular competition. *Nature* **599**, 645-649 (2021).
75. H. Kim, D. Lee, M. W. Jung, Signals for previous goal choice persist in the dorsomedial, but not dorsolateral striatum of rats. *J Neurosci* **33**, 52-63 (2013).
76. S. Yagishita, A. Hayashi-Takagi, G. C. Ellis-Davies, H. Urakubo, S. Ishii, H. Kasai, A critical time window for dopamine actions on the structural plasticity of dendritic spines. *Science* **345**, 1616-1620 (2014).
77. E. S. Her, N. Huh, J. Kim, M. W. Jung, Neuronal activity in dorsomedial and dorsolateral striatum under the requirement for temporal credit assignment. *Sci Rep* **6**, 27056 (2016).
78. J. A. Willett, J. Cao, A. Johnson, O. H. Patel, D. M. Dorris, J. Meitzen, The estrous cycle modulates rat caudate-putamen medium spiny neuron physiology. *The European journal of neuroscience* **52**, 2737-2755 (2020).
79. D. E. Oorschot, The percentage of interneurons in the dorsal striatum of the rat, cat, monkey and human: A critique of the evidence. *Basal Ganglia* **3**, 19-24 (2013).
80. T. A. Shnitko, S. W. Gonzales, N. Newman, K. A. Grant, Behavioral flexibility in alcohol-drinking monkeys: The morning after. *Alcohol Clin Exp Res* **44**, 729-737 (2020).
81. S. M. Groman, K. M. Rich, N. J. Smith, D. Lee, J. R. Taylor, Chronic exposure to methamphetamine disrupts reinforcement-based decision making in rats. *Neuropsychopharmacology* **43**, 770-780 (2018).
82. V. M. Brown, L. Zhu, A. Solway, J. M. Wang, K. L. McCurry, B. King-Casas, P. H. Chiu, Reinforcement learning disruptions in individuals with depression and sensitivity to symptom change following cognitive behavioral therapy. *JAMA Psychiatry* **78**, 1113-1122 (2021).

83. Y. Vandaele, N. R. Mahajan, D. J. Ottenheimer, J. M. Richard, S. P. Mysore, P. H. Janak, Distinct recruitment of dorsomedial and dorsolateral striatum erodes with extended training. *Elife* **8**, e49536 (2019).
84. A. Wiehler, K. Chakroun, J. Peters, Attenuated directed exploration during reinforcement learning in gambling disorder. *J Neurosci* **41**, 2512-2522 (2021).

Acknowledgements

We thank Nikhila Kalapatapu, Tina Feng, and Jeniffer Min for assisting on a subset of animal experiments.

Funding:

National Institutes of Health grant R01AA026306 (PHJ)
National Institutes of Health grant R01AA031609 (PHJ)
National Institutes of Health grant R01DA035943 (PHJ)
Intramural Research Program of the National Institute of Mental Health ZIAMH002983 (AJL)
JHU Kavli NDI Fellowship (YC)

Author contributions:
Yifeng Cheng: Writing – original draft, Conceptualization, Investigation, Writing – review & editing, Methodology, Data curation, Validataion, Formal analysis, Software, Project administration, Visualization
Patricia H. Janak: Conceptualization, Writing – review & editing, Methodology, Resources, Funding acquisition, Validation, Supervision, Project administration
Angela J. Langdon: Writing – review & editing, Methodology, Funding acquisition, Validation, Formal analysis, Software
Robin Magnard: Investigation, Writing – review & editing
Daeyeol Lee: Writing – review & editing, Methodology

Competing interests: The authors declare that they have no competing interests.

Data and materials availability: All data needed to evaluate the conclusions in thepaper are present in the paper and/or the Supplementary Materials. Data and code are available from Zendo https://doi.org/10.5281/zenodo.14188121.

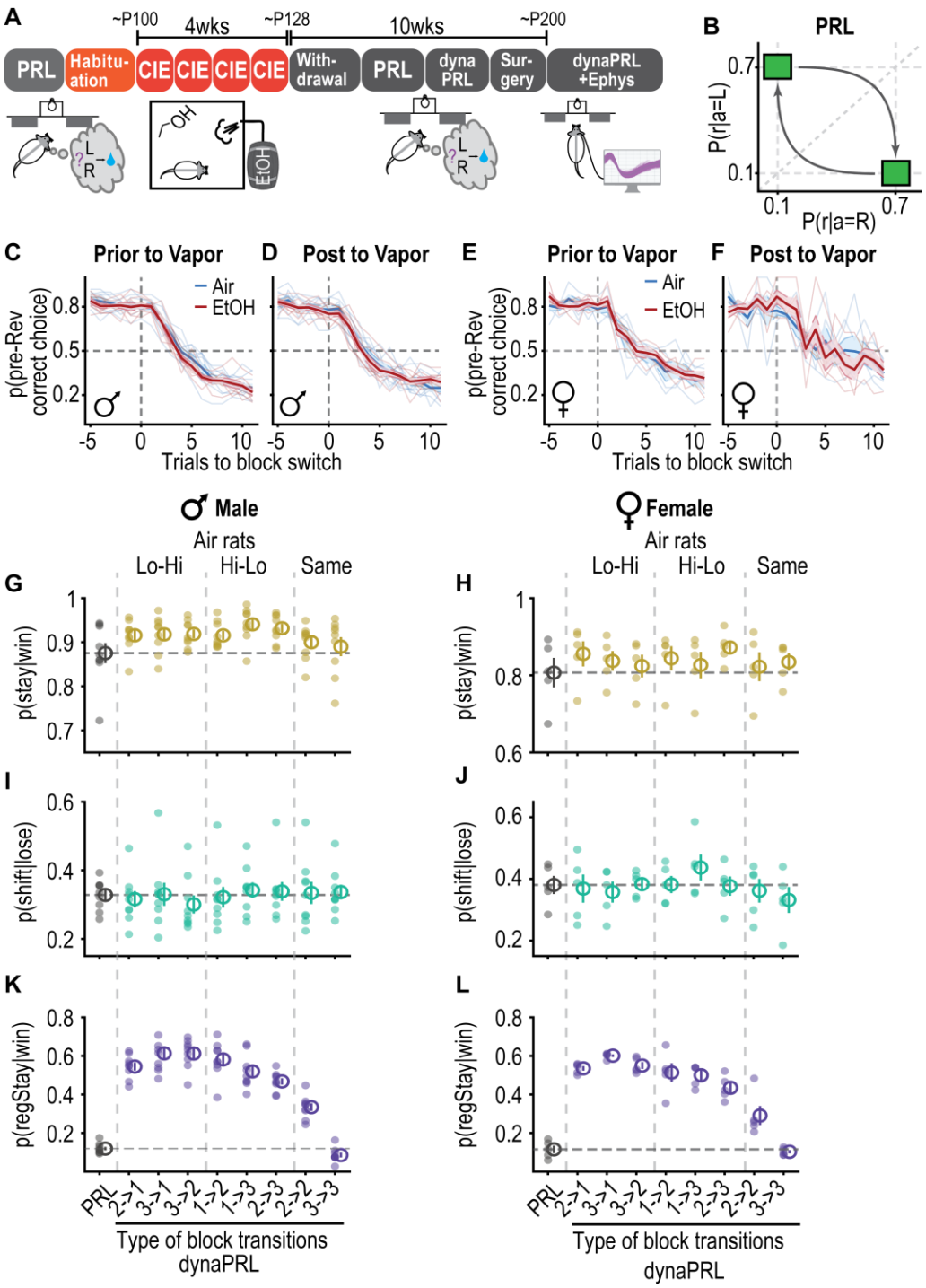

Figure S1. Protracted withdrawal from chronic ethanol exposure does not impair adaptive learning in traditional probabilistic reversal learning task. (**A**) Experimental timeline: Rats underwent training in a simple probabilistic reversal learning (PRL) task to counterbalance their behavior prior to 4 sessions habituation to the vapor chambers followed by a 4-week chronic ethanol vapor exposure (CIE) procedure. Following 10-15 days of withdrawal from CIE, rats were retrained with the PRL task and then introduced to a new task, the dynamic probabilistic reversal learning (dynaPRL) task. 16-channel drivable electrodes were implanted in dorsomedial

striatum of rats. After recovery and retraining, single-unit activity was recorded. (**B**) Choice reward probabilities for the PRL task. The reward probabilities associated with each lever, either 0.7 or 0.1, switched within the session. (**C,D**) Probability of choosing pre- block switch preferred lever before (C) and after (D) CIE vapor in males. N = 9 male air rats, 8 male CIE rats. (**E**,**F**) Probability of choosing pre- block switch preferred lever before (E) and after (F) CIE vapor in females. N = 5 female Air rats, 5 female CIE rats. Bold lines represent the group average and faded lines represent individual rats. Vertical dashed line indicates the last trial before block switch (t=0) for D-G. (**G**,**I**,**K**) For male rats, G) Probability of repeating the same choice (stay) after a reward (win); I) probability of switching choices (shift) after no reward (lose); and K) probability of repeating the choice preferred in the previous block (regressive stay, regStay) after a reward (win) on the last trial. These behaviors are observed during trials 2-9 immediately following a block switch in both the PRL and each block transition in the dynaPRL task. Dots represent individual rats in both air and EtOH groups; open circles next to the dots indicate the mean probability across rats, with vertical lines showing SEM. N = 8 male EtOH rats and 9 male air rats. (**H**,**J**,**L**) Similar to B-D for female rats H) Probability of repeating the same choice (stay) after a reward (win); J) probability of switching choices (shift) after no reward (lose); and L) probability of repeating the choice preferred in the previous block (regressive stay, regStay) after a reward (win) on the last trial.

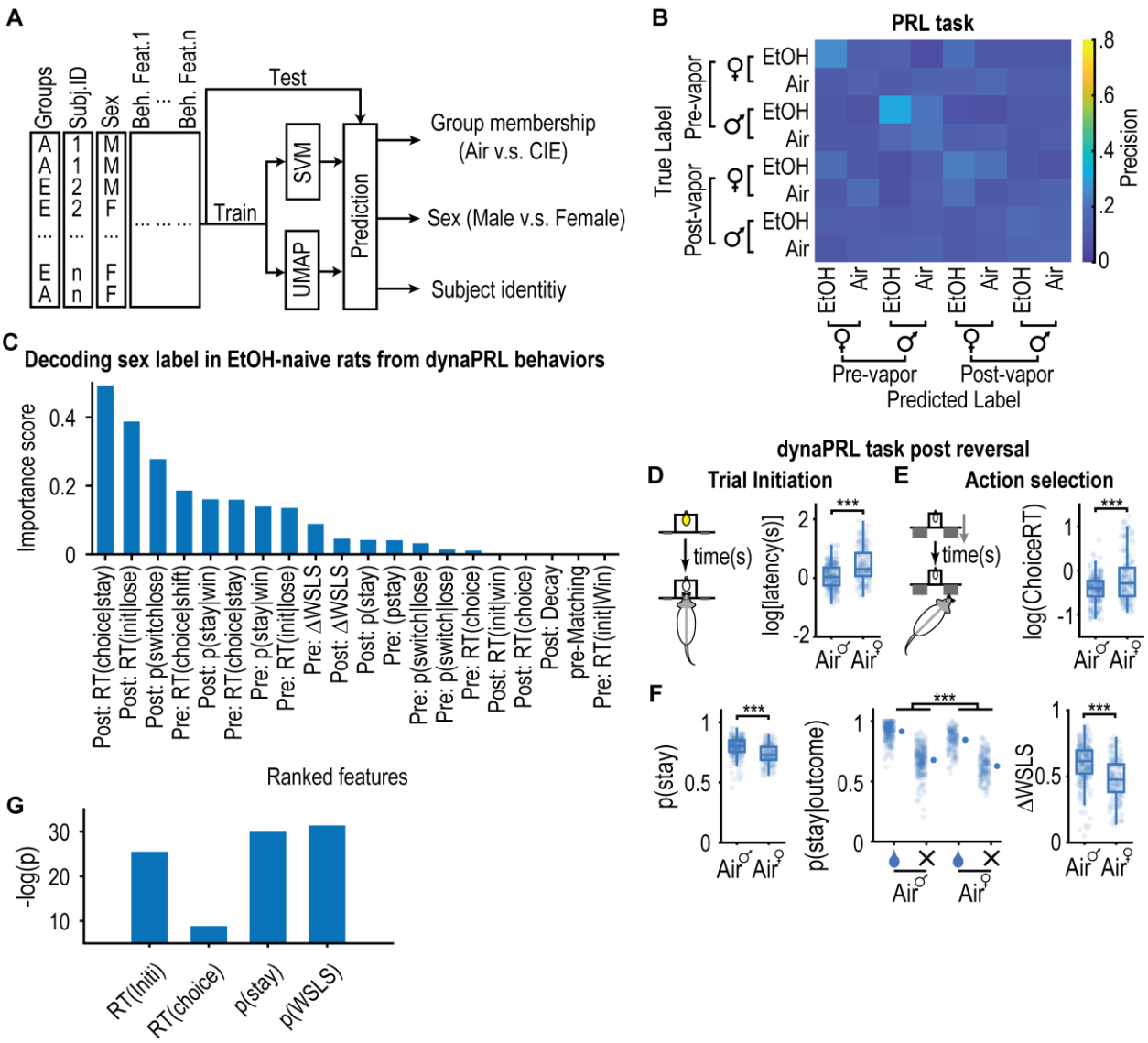

Figure S2. EtOH-exposed rats do not exhibit a distinct behavioral pattern in the standard PRL task and basal behavioral sex differences observed in the dynaPRL. (**A**) The diagram illustrates the classification analysis process. (**B**) Confusion matrix for the SVM multiclass classifier aggregating from 1000 iterations for decoding group membership (EtOH vs. Air), sex, and exposure conditions (pre- v.s. post-vapor) for N = 13 EtOH rats (8 male, 5 female) and 14 air controls (9 male, 5 female). Diagonal entries represent accurate predictions, while off-diagonal elements represent misclassifications. Classification precision is computed from [true positive rate/(true positive rate + false positive rate)]. *p < 0.05 indicates statistical significance determined through Monte Carlo tests. (**C**) Importance scores for each behavioral measurement (feature) used in SVM decoding to distinguish sex labels in EtOH-naïve (air only) rats. The features are ranked in descending order based on their importance scores. (**D**) Latency of trial initiation after block switch in male and female air rats during dynaPRL. ***p < 0.0001, Wilcoxon rank-sum test. (**E**) Latency of action selection after block switch male and female air rats during dynaPRL. ***p = 0.00015, Wilcoxon rank-sum test. (**F**) Stay probability (left panels), stay probability given reward (water drop) or no reward (X) on the last trial (middle panels), and difference of win-stay lose-switch probability (ΔWSLS; right panels) in male and female air rats

during the post-block switch phases of dynaPRL. Left panel, ***$p < 0.0001$, Wilcoxon rank-sum test. Middle panel, ***$p < 0.0001$, two-way mixed-effect ANOVA. Right panel, ***$p < 0.0001$, Wilcoxon rank-sum test. (**G**) Statistical effect, measured by the negative log p-value, comparing among behavioral measures in D-F. This analysis aimed to identify which behavioral measure had the strongest effect in distinguishing male and female rats within the air control groups. The results indicate that the difference in win-stay/lose-shift probability had the highest statistical effect, followed by the probability of staying, suggesting that choice strategy features are particularly powerful in differentiating sex in control groups.

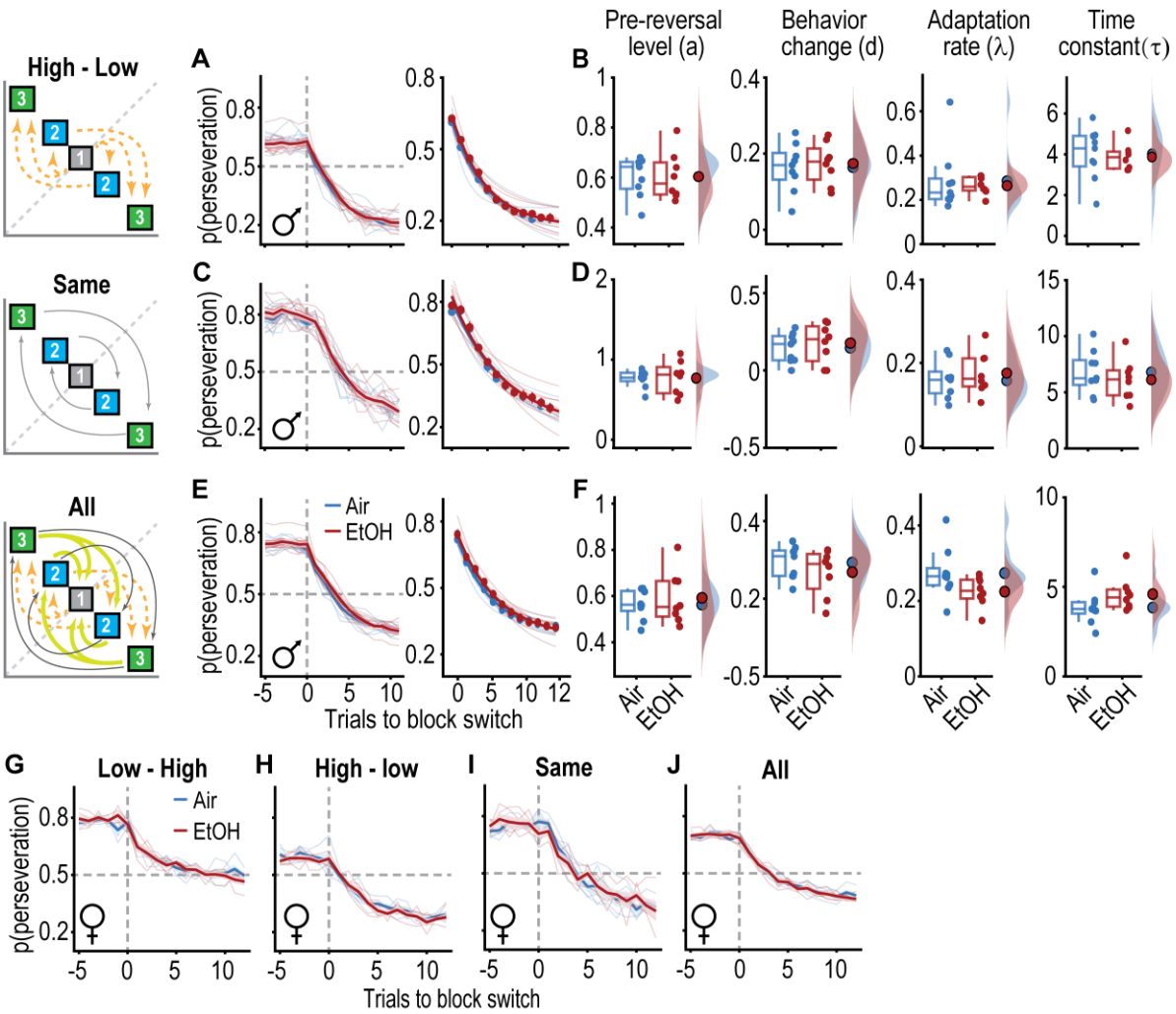

Figure S3. Prior EtOH exposure does not alter adaptive learning under low uncertainty in the dynaPRL task. (**A**,**C**,**E**) The probability of selecting the preferred lever before the block switch (left panel) and the performance estimated by the single exponential decay model for learning new action-outcome contingency (right panel) during transitions with A) High-to-Low uncertainty, C) Same, or E) transitions aggregated across all types in male rats. In the right panels, bold lines indicate the average model fit for the probability of selecting an action based on the pre-switch contingencies. In the right panels, dots represent the true mean data from A, C, and E, and faded lines illustrate model estimates of individual rat choice probability. **(B,D,F)** The estimated parameters' pre-block switch asymptotic value (pre-rev. level), a; magnitude of change in p(preservation) (behavior change), d, adaptation rate, λ, and time constant, τ, for the single exponential decay model during transitions with B) High-Low, D) Same, and F) transitions aggregated across all types in males. Dots represent individual rats. The box plot depicts the median, 25th, and 75th percentile of the parameter values for each group. Two-way mixed-effect ANOVA for A, C and E. Two-sample independent t test with two-tails for B, D and F. (**G**-**J**) Probability of selecting pre-switch preferred lever in G) transitions with Low-High, H) High-Low, and I) Same type transitions as well as transitions aggregated across all types in females. Bold lines indicate the average probability of selecting an action based on the pre-switch contingencies across rats. Two-way mixed-effect ANOVA for G-J. N = 13 EtOH rats (8 male, 5 female) and 14 air controls (9 male, 5 female).

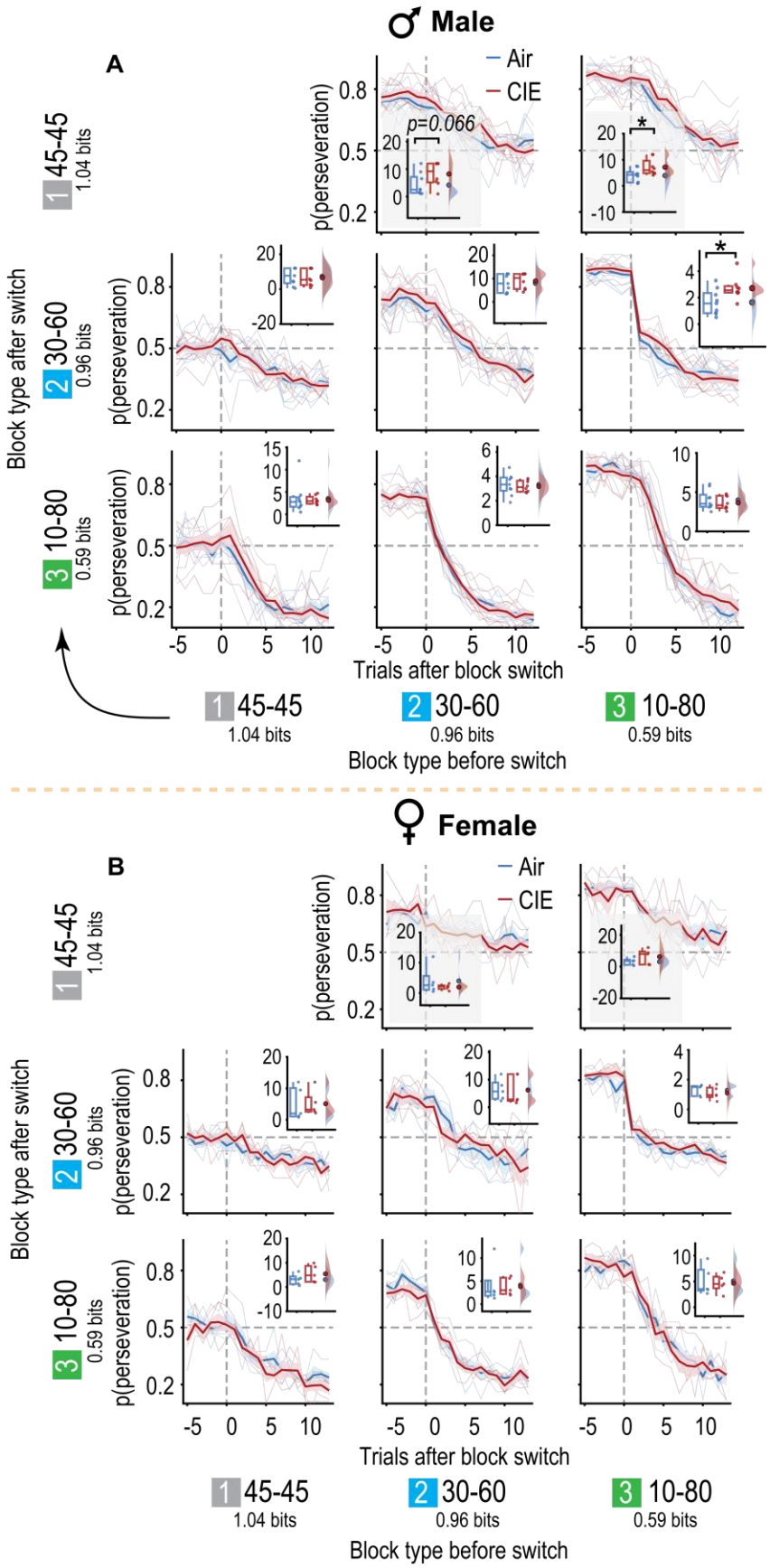
♂ Male
A
Air
CIE
p(perseveration)
p=0.066
*
1 45-45
1.04 bits
2 30-60
0.96 bits
3 10-80
0.59 bits
Block type after switch
Trials after block switch
Block type before switch
♀ Female
B

1133

Figure S4. Unexpected uncertainty modulates rats' choice behavior in the dynaPRL task. (**A**) Probability of male rats selecting the preferred lever before block switch for each individual block transition type. For unexpected uncertainty (sudden transitions), choice adaptation rates were quantified with exponential decay time constants. Male rats regardless group exhibited distinct time constants and EtOH-exposed males take a longer time to learning new action-reward probabilities when transitioning from low- to high-uncertainty blocks (e.g., block 3 → 2, 3 → 1, 2 → 1). For expected uncertainty (stable pre-switch behavior), choice probabilities were consistent across identical block types: 50% in the 45-45 block (no correct choice), 75% in the 60-30 block, and 83% in the 80-10 block, unaffected by EtOH exposure. However, EtOH exposure enhanced choice matching to global reward rates in blocks 2 and 3 for male rats, indicating a potential sex-dependent interaction between alcohol and expected uncertainty. Light lines represent individual rats, bold lines show the group average, and the inset displays time constants from an exponential decay model. The entropy of each block, indicating the level of expected uncertainty, is noted below each block label. Time constants were compared between groups using an independent t-test (*$p < 0.05$). N = 8 male EtOH rats and 9 male air rats. (**B**) Similar to males, female rats' probability of selecting the preferred lever was analyzed for each block transition type. Female rats exhibited distinct time constants in response to different types of unexpected uncertainty across transitions. Notably, EtOH exposure did not alter learning performance or choice probabilities in female rats. N = 5 female EtOH rats and 5 female air rats.

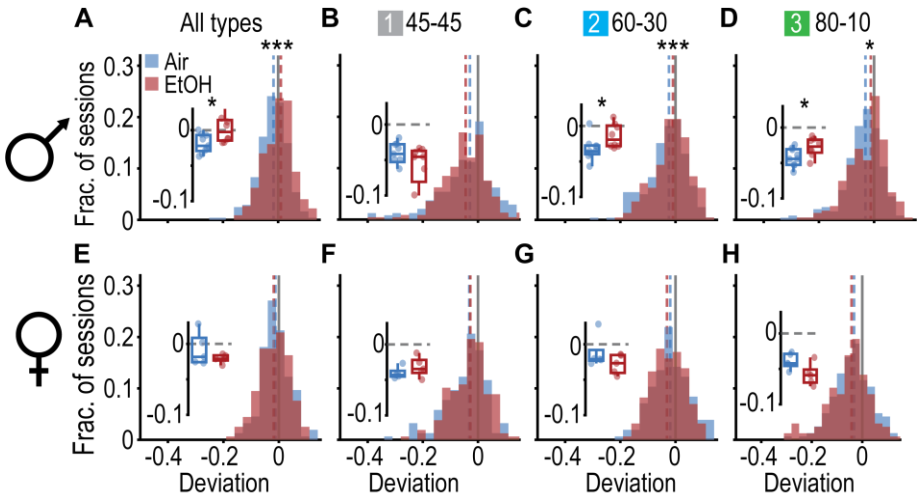

Figure S5. Prior EtOH exposure reduces deviation from matching choice behavior to local reward rate in males but not in females. (**A-D**) Histograms reveal higher matching scores (deviation of choice probability from the reward probability given the choice) in trials from A) blocks aggregating across all transition types, and C) low contrast (60-30), as well as D) high contrast (80-10) blocks, but not from B) neutral blocks (45-45), in EtOH rats compared to air controls. Vertical blue and red dashed lines represent the median deviation from matching, while the vertical grey solid lines represent perfect matching (0 deviation of choice probability to reward probability given the choice). The inset panels depict the mean deviation score averaged for each EtOH rat and air control, with each dot representing a rat. The horizontal dashed line indicates perfect matching. (**E-H**) Similar to A-D, histograms show no difference in matching scores in E) all, F) neutral, G) low contrast, and H) high contrast type blocks. *$p < 0.05$ and ***$p < 0.001$. The Mann-Whitney test was used for comparisons in histograms A-H. For all inset panels in A-H, a two-tailed independent two-sample t-test was applied. N = 13 EtOH rats (8 male, 5 female) and 14 air controls (9 male, 5 female).

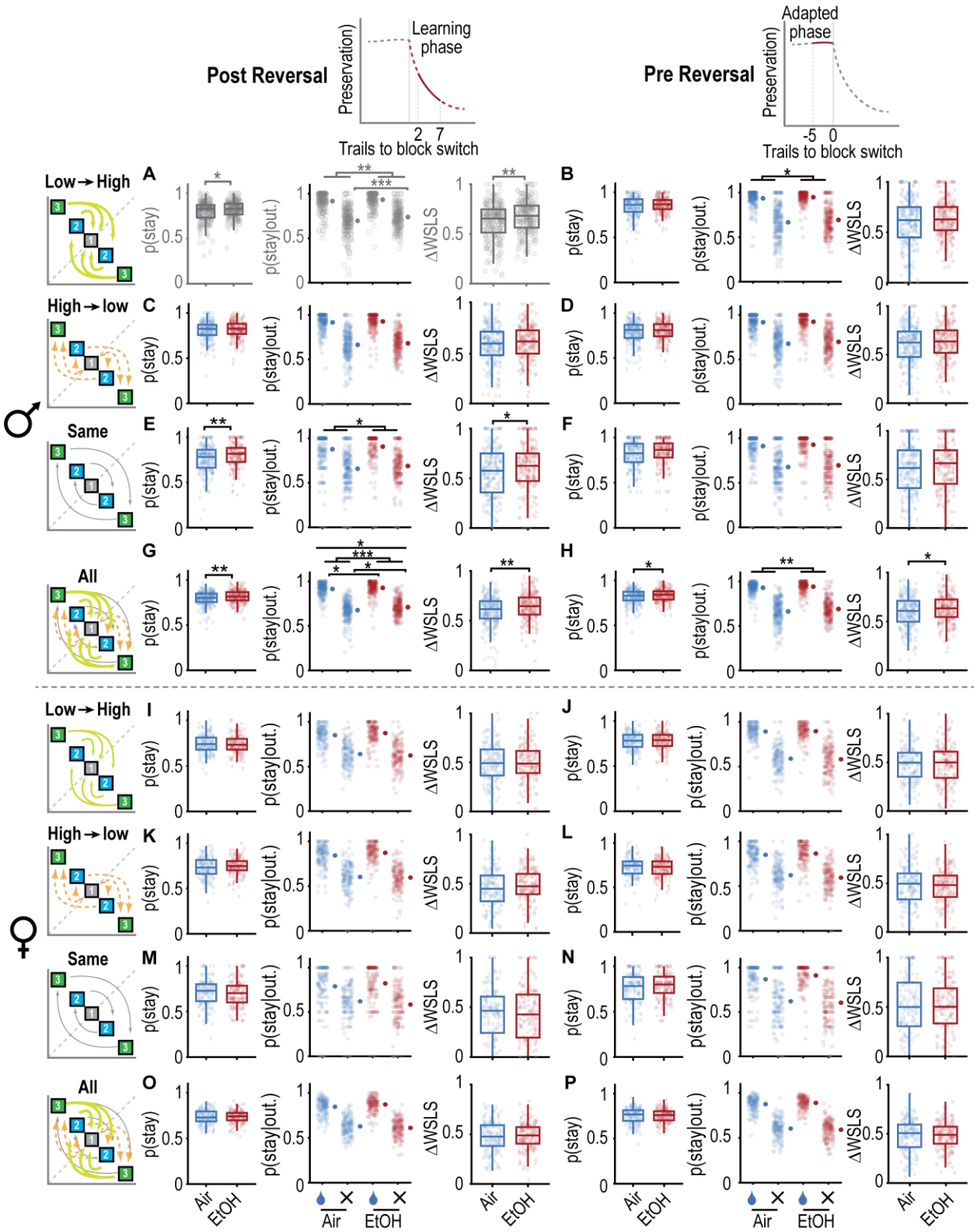

Figure S6. Stay probabilities pre- and post-block switch under various cognitive challenge conditions. (**A-H**) Stay probability (left panels), Stay probability given reward (water drop) or no reward (X) on the last trial (middle panels), and difference of win-stay lose-switch probability

(ΔWSLS; right panels) in post-block switch (A, C, E, and G) and pre- block switch (B, D, F, and H) phases during various uncertainty conditions in males. Data in A is duplicated from Figures 2H-2J. (**I-P**) Stay probability (left panels), conditional stay probability (middle panels), and difference of win-stay lose-switch probability (ΔWSLS; right panels) in pre- block switch (I, K, M, and O) and post- block switch (J, L, N, and P) phases during various uncertainty conditions in females. Dots in all left and right panels represent individual sessions in air and EtOH groups. In all middle panels, dots next to the scatter plot represent the mean of data. Standard errors are vertical lines but are too small to visualize on the graph. *$p < 0.05$, **$p < 0.01$, and **$p < 0.001$, Wilcoxon rank-sum test for the left and right panels in A-P; Two-way mixed-effect ANOVA for the middle panels in A-P. N = 241 sessions from 9 male air rats and 229 sessions from 8 male EtOH rats.

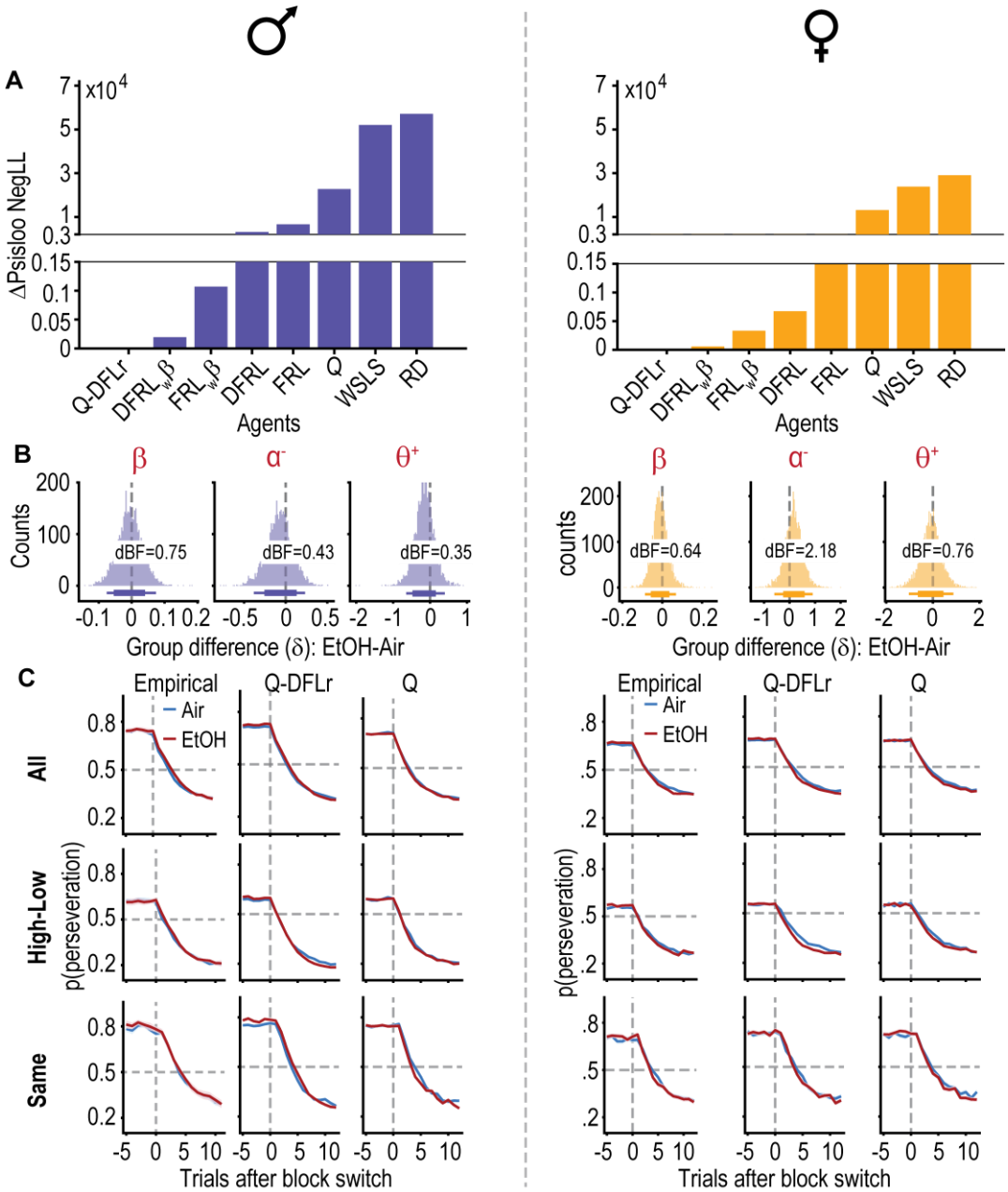

Figure S7. Fit of reinforcement learning models to trial-by-trial data from the dynaPRL task for male and female rats. (**A**) The bar plot shows the difference of Pareto-smoothed importance sampling (PSIS) with leave-one-out (LOO) negative likelihood (ΔPsisloo NegLL) between candidate models and the best fitting model, Q learning model with differential learning rate (Q-DFLr), which is left-most on the x-axis. (**B**) Hamiltonian Markov chain Monte Carlo (HMC)-sampled posterior densities of group difference, δ, from the Q-DFLr model, representing differences between EtOH- and air-exposed rats in inverse temperature (β in the left panel), negative feedback-mediated learning rates (α^- in the middle panel), and positive feedback-mediated forgetting rates (θ^+ in the right panel), across group-level hyperparameters. Bottom horizontal lines represent the 80% and 95% highest density interval (HDI). dBF: directed Bayes factor. Posterior densities aggregated from 1000 times Monte Carol sampling. (**C**) Comparison of empirical data with Q-DFLr and standard Q learning models. Choice probability of the

initially preferred lever in all, High-low, and Same transitions. Empirical data are reproduced from Figure 1G for male, ♂, and from Figure S3 for female, ♂, respectively. Simulated data generated using the best-fitting parameters from Q-DFLr and Q models, respectively. Each line represents an average of 20 simulations. Left panels in A-C are data from males (♂) and right panels in A-C are data from females (♀).

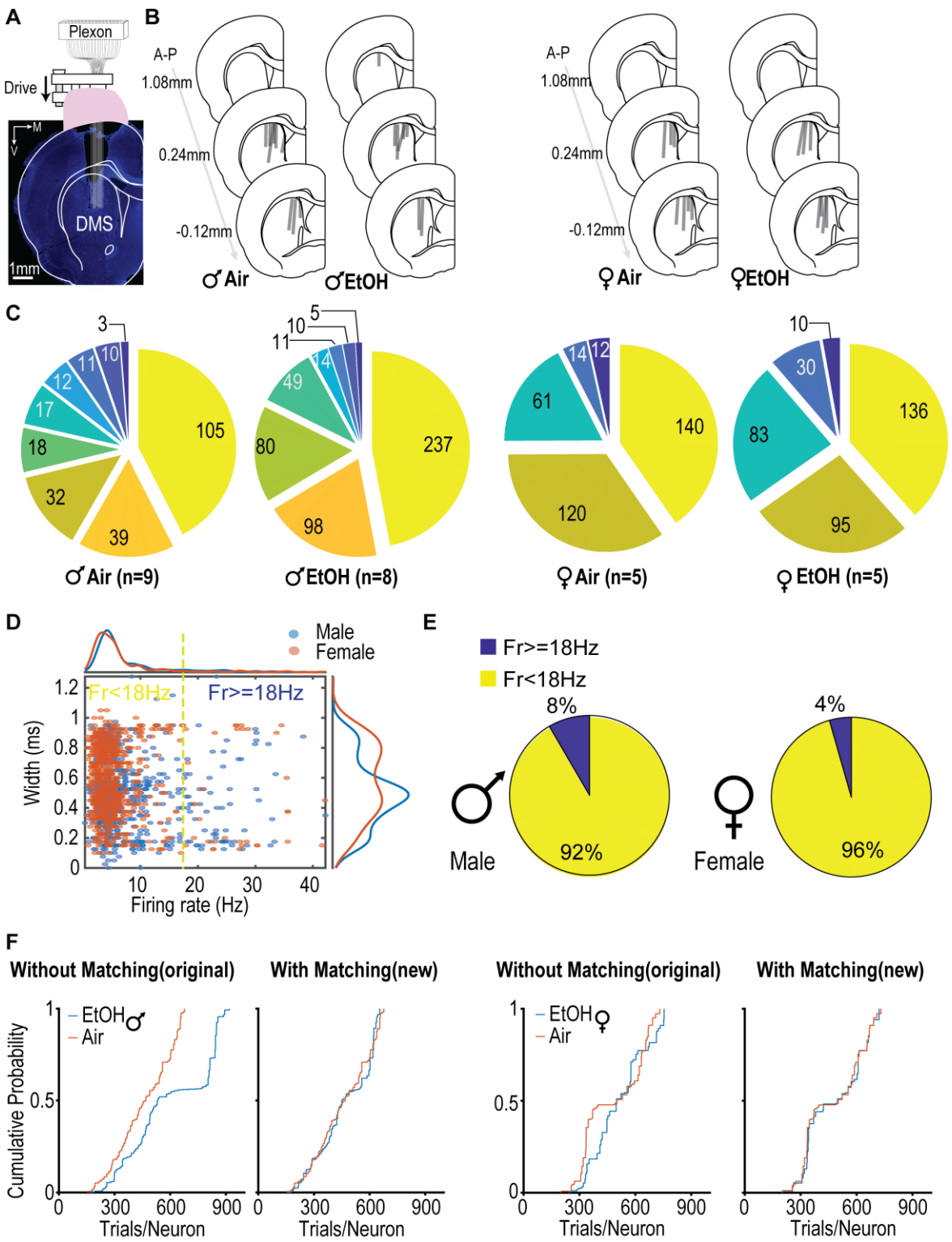

Figure S8. Single unit recording in the dorsomedial striatum (DMS). (**A**) The diagram illustrates a drivable electrode consisting of 16 tungsten wires connected to a Plexon headstage, which is implanted in the dorsomedial striatum (DMS). (**B**) Electrode placement for each male (♂) and female (♀) animal, denoted by grey lines. (**C**) Pie charts show the aggregate count of neurons recorded from each rat. A two-sample Kolmogorov-Smirnov test revealed no significant

difference in the distribution of recorded neurons between EtOH and Air groups for both males and females. (**D**) Scatter plot of average firing rate across the entire session and spike widths for all recorded units in both male and female rats. Histograms to the top and right display the normalized distribution density of the units' mean firing rate and spike width, respectively. (**E**) Pie charts of proportion of fast-spiking neurons (firing rate, Fr $\geqslant$ 18 Hz) and slow-spiking neurons (firing rate, Fr < 18 Hz) in male (left) and female (right) rats. (**F**) Cumulative probability distributions illustrate the number of trials for each recorded neuron before (left) and after (right) trial-matching. This matching was conducted between EtOH and air groups, separately for males and females.

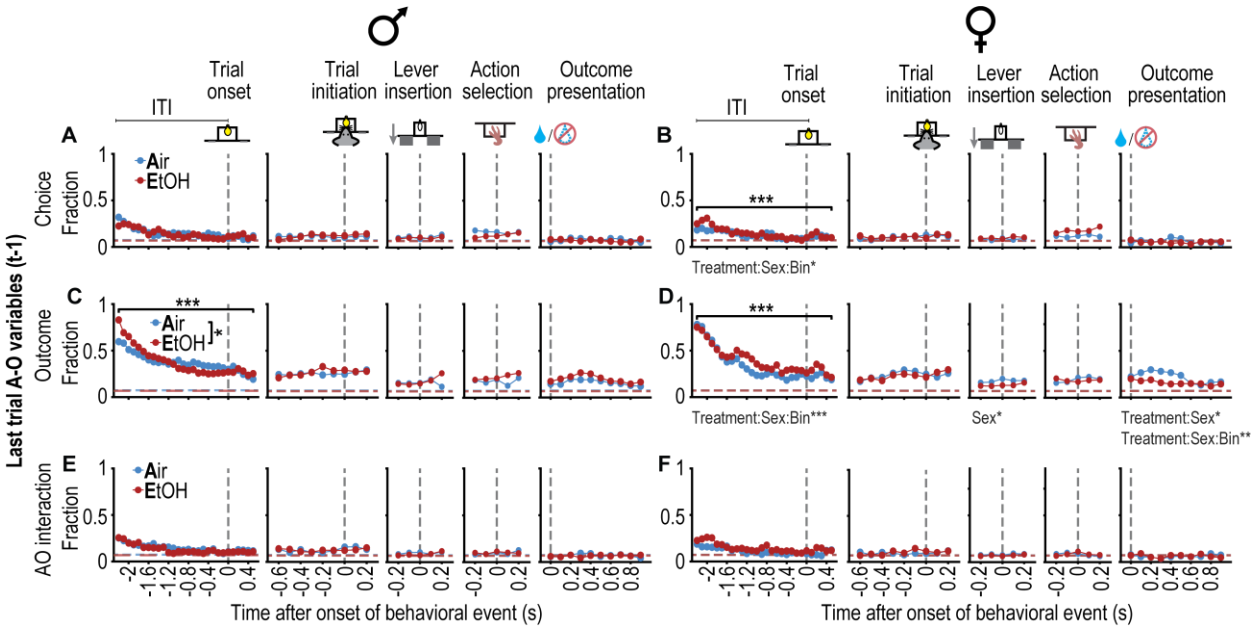

Figure S9. EtOH pre-exposure differentially alters the striatal representation of choice and outcome signals from the previous trial in male and female rats. (**A-F**) Fraction of neurons in males and females showing significant modulation by choice (A for males, B for females), outcome (C for males, D for females), and the interaction of choice and outcome (E for males, F for females) from the previous trial, around behavioral events such as trial onset, trial initiation, lever insertion, lever press, and outcome report. Vertical gray dashed lines mark the onset of each behavioral event. Horizontal blue and red dashed lines indicate the chance level for the air and EtOH groups, respectively. In A, during action selection, $p = 0.018$ main effect of treatment and $p = 0.02$. In B, during trial onset, $p = 0.0007$ interaction between treatment and time and $p = 0.02$ interaction among treatment, sex and time. In C, during trial onset, $p = 0.01$ main effect of treatment and $p < 0.0001$ interaction between treatment and time. In C, during lever insertion, $p = 0.049$ for main effect of treatment and $p = 0.00025$ interaction between treatment and time. In D, during trial onset, $p < 0.0001$ interaction between treatment and time and $p < 0.0001$ interaction between treatment, sex and time. In D, during lever insertion, $p = 0.022$ main effect of sex. In D, during outcome presentation, $p = 0.016$ interaction between treatment and sex and $p = 0.0069$ interaction among treatment, sex and time. The horizontal dashed lines indicate the chance level (binomial test, $\alpha = 0.05$). Logistic regression with Generalized Linear Mixed-Effect Model for A-F. n = 247 neurons from 9 air male rats, 504 neurons from 8 EtOH male rats, 347 neurons from 5 air female rats, and 354 neurons from 5 EtOH female rats.

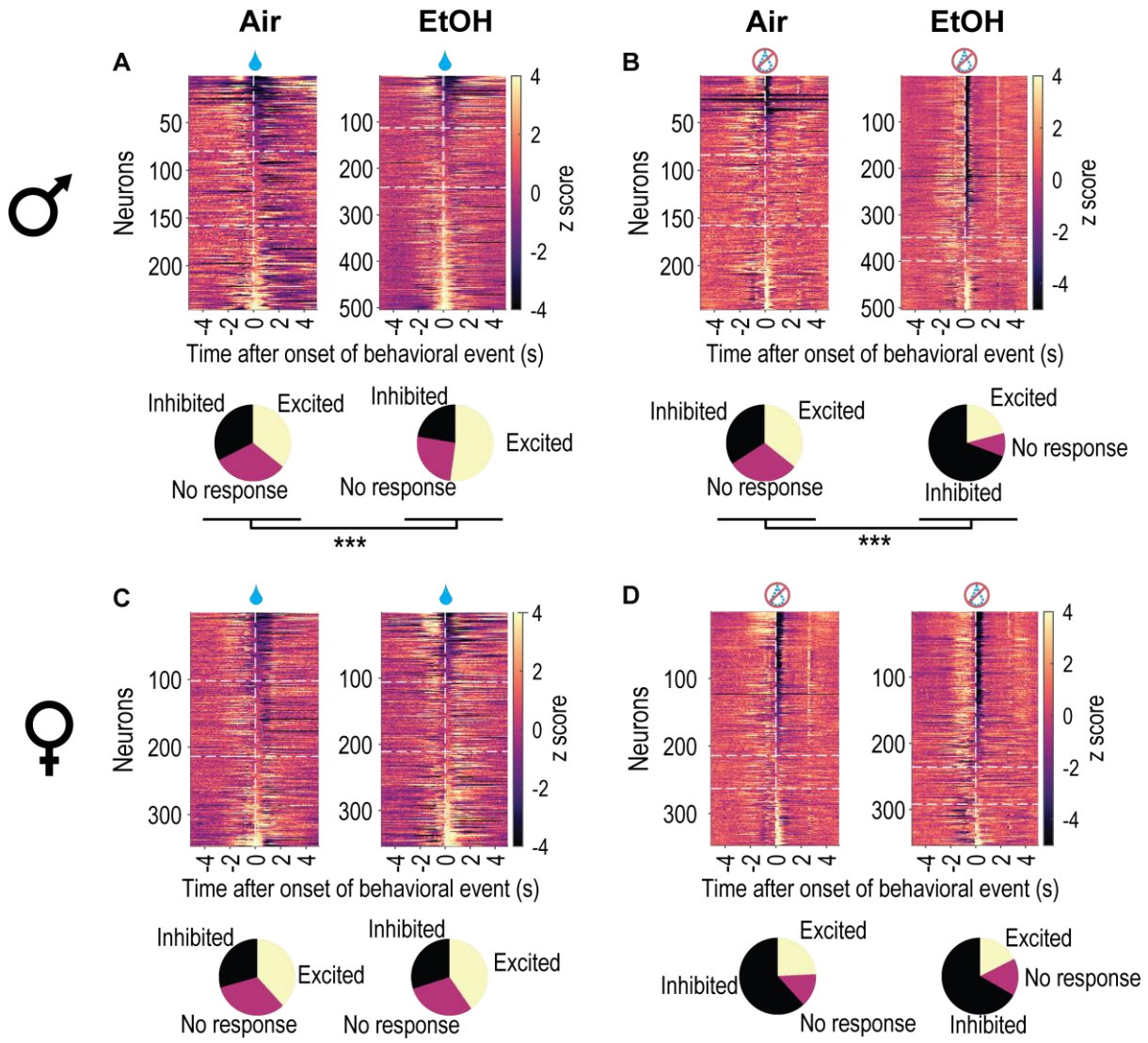

Figure S10. EtOH pre-exposure alters striatal firing in response to rewarded and unrewarded outcomes in males. (**A,B**) The heatmaps depict z-scored neuronal firing rates from male rats before and after A) reward delivery or B) unrewarded outcome presentation. ***p < 0.001, Chi-squared test. n = 247 units from 9 male air rats, 504 units from 8 male EtOH rats. (**C**,**D**) The heatmaps depict z-scored neuronal firing rates from female rats before and after C) reward delivery or D) unrewarded outcome presentation. Vertical dashed lines indicate the onset of reward (A,C) and unrewarded (C,D) outcomes. Neurons are sorted based on their peak z-scored firing rate averaged between 100 ms and 400 ms after the reward (A,C) or unrewarded outcome (B,D) onset. Horizontal lines demarcate subgroups of neurons that are significantly excited (top section), inhibited (bottom section), or non-responsive (middle section) to the reward for A-D. The bottom pie chart depicts the proportion of neurons in each response category for A-D. n = 347 neurons from 5 air female rats, and 354 neurons from 5 EtOH female rats.

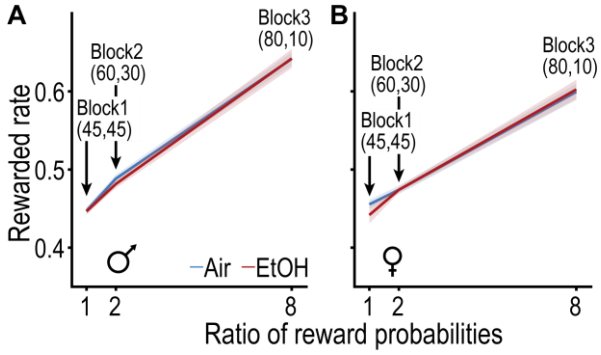

Figure S11. Reward rate as an indicator of block identity. (**A-B**) Reward rates (ratio of rewarded trials to total trials) linearly increase in correlation with the reward probability ratios, ranging from block 1 (45:45) to block 3 (80:10) for both A) males and B) females. Pearson correlation. N = 13 EtOH rats (8 males, 5 females) and 14 air controls (9 males, 5 females).

Table S1. Features used in SVM classification.

Feature ID	Phase relative to block switch	Feature full name
#1	Prior to block switch (pre)	Reversal decay
#2		Stay probability
#3		Stay probability given win
#4		Stay probability given lose
#5		Difference between win-stay and lose-shift probabilities
#6		Logarithmic transformed choice latency
#7		Logarithmic transformed choice latency given stay
#8		Logarithmic transformed choice latency given switch
#9		Logarithmic transformed trial initiation latency given win
#10		Logarithmic transformed trial initiation latency given lose
#11	After block switch (post)	Matching score
#12		Stay probability
#13		Stay probability given win
#14		Stay probability given lose
#15		Difference between win-stay and lose-shift probabilities
#16		Logarithmic transformed choice latency
#17		Logarithmic transformed choice latency given stay
#18		Logarithmic transformed choice latency given switch
#19		Logarithmic transformed trial initiation latency given win
#20		Logarithmic transformed trial initiation latency given lose

Behavioral features include measurements from trials before and after block switches averaged within sessions.